DESIGN PROTOCOLS AND ANALYTICAL STRATEGIES

THAT INCORPORATE STRUCTURAL RELIABILITY MODELS

Final Report

Principal Investigator:
Professor Stephen F. Duffy PhD, PE

Reporting Period:
January 19, 1996 - January 18, 1997

Cleveland State University
1983 East 24th Street
Cleveland, Ohio 44115

Grant Number:
NASA Cooperative Agreement NCC 3-448

ATTACHED SUMMARY

LeRC - GNTR

Section I - Description of the Problem that Motivated the Technology Development

Ceramic matrix composites (CMC) and intermetallic materials (e.g., single crystal nickel aluminide) are high performance materials that exhibit attractive mechanical, thermal, and chemical properties. These materials are critically important in advancing certain performance aspects of gas turbine engines. From an aerospace engineer's perspective the new generation of ceramic composites and intermetallics offers a significant potential for raising the thrust/weight ratio and reducing NO_x emissions of gas turbine engines. These aspects have increased interest in utilizing these materials in the hot sections of turbine engines. However, as these materials evolve and their performance characteristics improve a persistent need exists for state-of-the-art analytical methods that predict the response of components fabricated from CMC and intermetallic material systems. This need provided the motivation for the technology developed under this research effort.

Continuous ceramic fiber composites exhibit an increase in work of fracture, which allows for "graceful" rather than catastrophic failure. When loaded in the fiber direction, these composites retain substantial strength capacity beyond the initiation of transverse matrix cracking despite the fact that neither of its constituents would exhibit such behavior if tested alone. As additional load is applied beyond first matrix cracking, the matrix tends to break in a series of cracks bridged by the ceramic fibers. Any additional load is born increasingly by the fibers until the ultimate strength of the composite is reached. Thus modeling efforts supported under this research effort have focused on predicting this sort of behavior.

For single crystal intermetallics the issues that motivated the technology development involved questions relating to material behavior and component design. Thus the research effort supported by this grant had to determine the statistical nature and source of fracture in a high strength, NiAl single crystal turbine blade material; map a simplistic failure strength envelope of the material; develop a statistically based reliability computer algorithm; verify the reliability model and computer algorithm; and model stator vanes for rig tests.

Thus establishing design protocols that enable the engineer to analyze and predict the mechanical behavior of ceramic composites and intermetallics would mitigate the prototype (trial and

error) approach currently used by the engineering community. The primary objective of the research effort supported by this short term grant is the continued creation of enabling technologies for the macroanalysis of components fabricated from ceramic composites and intermetallic material systems. The creation of enabling technologies aids in shortening the product development cycle of components fabricated from the new high technology materials.

ATTACHED SUMMARY

LeRC - GNTR

Section II - Description of the New Technology that was Developed

The majority of the technology developments relating to ceramic matrix composites was reported on in a final report for the NASA grant that preceded this effort (NCC 3-310). The discussion here focuses on the efforts relating to intermetallic technology that occurred under the short duration of this research project. The new technology pertaining to the nickel aluminide (NiAl) intermetallic primarily focused on expanding the data base of mechanical properties. In addition, preliminary work began on developing aspects of a multiaxial reliability model for this material.

The nickel aluminide (NiAl) material under consideration is very brittle and highly anisotropic (Young's modulus varies from 95 to 271 GPa, depending on the direction of crystallization). Since the material is brittle and highly anisotropic the statistical nature and source of fracture was studied using flexural test specimens (ref. 1) fabricated from small billets (25 x 50 x 100 mm) where the direction of crystallization in each billet was identified prior to specimen preparation. Use of flexural test specimens allowed a maximum number of test specimens to be fabricated from a given region of a billet. This permitted the determination of billet-to-billet, and within billet variation of ultimate strengths. Both factors will affect stator vane reliability. Further, in contrast to tensile testing, flexural testing allows the location the failure site within a specimen since the asymmetry of flexural loading results in an identifiable shattering pattern.

Two basic types of flaws are typically encountered in brittle materials: surface defects and volumetric defects. Volumetric defects include large grains, pores, agglomerates and inclusions, while surface defects include exposed volume defects (e.g. a pore machined open) and machining or handling damage occurring during specimen/component fabrication (ref. 2). Flexural strength results to date indicate that the material exhibits a wide dispersion in strength which can be characterized by Weibull statistics. Failure origins were identified in 25 of 27 specimens tested. In all cases failure occurred from singular, coarse Hf-rich or Hf-Ni-Al particles.

Brittle materials frequently fail from a single, strength limiting origin or region within the material due to the low toughness and low ductility. The strength of such a system is thus governed by the weakest-link within the system and thus dependent on the surface area and volume stressed during

testing. Weibull statistics (ref. 3 and ref. 4) are commonly used for reliability analysis of components fabricated from these types of materials. The calculated failure probability is dependent on the stress state and the material properties of the component. However, this procedure is inadequate to describe experimental data obtained from test specimens fabricated from anisotropic materials. The use of NiAl in the fabrication of structural components used in gas turbine engines requires a rigorous reliability theory. Specifically, a reliability theory should combine linear elastic fracture mechanics with established statistical failure theories. Several isotropic theories applicable to ceramics and glasses have been incorporated into the public domain computer algorithm entitled Ceramics Analysis and Reliability Evaluation of Structures (CARES) (ref. 5) code developed at NASA Lewis. This algorithm, when combined with a finite element method (FEM) stress analysis, calculates fast fracture probability of a brittle, monolithic structural component. An effort to modify the algorithm to account for the anisotropy of single crystal NiAl began under this short duration research effort. Future research efforts will focus on verifying the modeling efforts that began here.

Verification of a failure theory can be accomplished via measurement of points on the failure envelope and comparison to predictions by the model and code. Each point on the failure envelope represents a stress state and thus can be measured experimentally for a given material via strength testing with various geometries. Strength tests planned for verification work include flexure (3 and 4-point), pure tension, pure compression, torsion and biaxial flexure. To date, uniaxial and biaxial flexural tests have been conducted, and a torsion specimen is being designed and verified relative to handbook solutions. Since the NiAl material exhibits elastic anisotropy and variation in fracture toughness with orientation (ref. 6), several orientations will be considered in strength testing.

References

1. ASTM C 1161-90 "Standard Test Method for Flexural Strength of Advanced Ceramics at Ambient Temperature," American Society for Testing and Materials Annual Book of Standards, Vol. 15.01, 1990, pp. 333-339.

2. "Fractography and Characterization of Fracture Origins in Advanced Structural Ceramics," MIL-HDBK-790, (July, 1992).

3. W. Weibull, "A Statistical Theory of the Strength of Materials," Ingeniors Vetenskaps Akademien Handlinger, No. 151, 1939.

4. J. P. Gyekenyesi, "SCARE: A Postprocessor Program to MSC/NASTRAN for Reliability Analysis of Structural Ceramic Components," J. Eng. Gas Turbine Power, Vol. 108, No. 3, July, 1986, pp. 540-546.

5. N. Nemeth, J. Manderscheid, J. Gyekenyesi, "CARES Users and Programmers Manual," NASA Technical Paper TP2916, 1990.

6. K. Chang, R, Darolia and H. Lipsitt, "Cleavage Fracture in B2 Aluminides," *Acta Metall.* Vol. 40, No. 10, 1992, pp. 2727-2737.

ATTACHED SUMMARY

LeRC - GNTR

Section III - Unique and Novel Features of the Technology & Results/Benefits of Application

The primary objective of the principal investigator's efforts is the creation of enabling technologies for the macro-analysis of aerospace components. During the duration of this research grant the technical efforts of the principal investigator were made a part of a cooperative agreement with General Electric Aircraft Engines and NASA LeRC. Specifically, the principal investigator guided the development of a design analysis which focused on modeling a GEAE stator vanes fabricated from a nickel aluminide intermetallic material. These vanes will be inserted in a rig test sometime in the near future. The modeling has been done via the finite element method, and the CARES algorithm will be utilized in order to predict component reliability. The modeling effort is described below. The enabling technologies developed under this research effort and past research efforts will aid in shortening the product development. The results/benefits of application are compiled in the following summary of this research project.

ACCOMPLISHMENTS DURING YEAR 1995-1996

During the past year the principal investigator has continued to guide the development of a design analysis as part of a cooperative agreement with General Electric Aircraft Engines. This effort is focused on modifying the CARES reliability algorithm for use in the design of engine components fabricated from NiAl. This intermetallic material will be utilized in single crystal form and it exhibits brittle behavior at lower service temperatures. In addition, the brittle strength of this material exhibits stochastic behavior, i.e., the ultimate strength is a random variable. The design approach advocates the following:

- Determination of the statistical nature and source of fracture in a high strength, NiAl single crystal turbine blade material;
- defining a phenomenological failure strength envelope for the material;
- developing a computer algorithm for statistically based reliability models;
- and developing analytical models of turbine blades and vanes for use in test bed engines.

From these preliminary tests it was concluded that the ultimate strength of this material could be adequately modeled using weakest-link reliability models (often referred to as Weibull analysis in the ceramics literature). The application of reliability theory to this particular material required the modification of current models (which assume isotropic material behavior) to account for anisotropic failure behavior. Several isotropic theories applicable to ceramics and glasses have been incorporated into a computer algorithm entitled Ceramics Analysis and Reliability Evaluation of Structures (CARES) developed under previous funding of this grant. This algorithm allows for anisotropic material behavior, however, a reliability model must be tailored to the NiAl material being analyzed in this project Work began on this aspect of the project in last quarter the grant period and is unfinished at the time of the premature close-out of this cooperative work agreement. Note that GE/AEBG provided researchers supported under this grant with a finite element model of a turbine blade which will be used in a future rig test. This model will be utilized in revamping the CARES algorithm.

The principal investigator also organized a session for the ASME Biennial Conference on Reliability, Stress Analysis, and Failure Prevention. This conference was held in Boston, Massachusetts. The session was entitled "Fatigue and Creep of Materials." In addition the principal investigator organized a session for the ASME/IGTI International Gas Turbine and Aeroengine Congress & Exposition. This conference was held in Birmingham, England. The session was entitled "Life Prediction Methodologies: Ceramic Materials."

Conference Sessions Organized 1995-1996:

1. "Fatigue and Creep of Materials," Session #RSAFP - 2; 11th Biennial Conference on Reliability, Stress Analysis, & Failure Prevention; S.F. Duffy (chair); 17-20 September 1995; Boston, Massachusetts.

2. "Life Prediction Methodologies Ceramic Materials," Session # - International Gas Turbine and Aeroengine Congress & Exposition; S.F. Duffy (chair) J.P. Gyekenyesi (vice-chair); 5-8 June 1996; Birmingham, U.K.

Awards 1995-1996:

1. NASA Lewis Awareness Team Recognition - member of the HSR (High Speed Research) Phase I Team (November 1975)

ATTACHED SUMMARY

LeRC -GNTR

Section IV - Utilization of New Technology in Non-Aerospace Applications

The technology developed under this research effort has not been applied to non-aerospace applications.

ATTACHED SUMMARY

LeRC -GNTR

Section V - Additional Documentation

Publications:

1. "Reliability Analysis of Single Crystal NiAl Turbine Blades," J.L Palko, S.F. Duffy, J.A. Salem, R.D. Noebe, F. Holland, D.R. Wheeler, P.K. Wright, HITEMP Review 1994, Advanced High Temperature Engine Materials Technology Program, NASA CP-10146, Cleveland, Oh., pp. 56-1 through 56-11, October, 1994.

2. "Design with Brittle Materials," S.F. Duffy and L.A. Janosik, to appear in Engineered Materials Handbook: Volume 20 Material Selection and Design, G. Dieter, volume chair, ASM International

RELIABILITY ANALYSIS OF SINGLE CRYSTAL NiAl TURBINE BLADES

JOSEPH PALKO[1], Stephen Duffy[1]
Cleveland State University
Cleveland,Ohio

P. Kennard Wright
General Electric Aircraft Engine Co.
Cincinnati, Ohio

Jonathan Salem, Ronald Noebe, Donald R. Wheeler and Fred Holland
NASA Lewis Research Center
Cleveland, Ohio

Introduction

As part of a co-operative agreement with General Electric Aircraft Engines (GEAE), NASA LeRC is modifying and validating the Ceramic Analysis and Reliability Evaluation of Structures (CARES ref. 1) algorithm for use in design of components made of high strength NiAl based intermetallic materials.

NiAl single crystal alloys are being actively investigated by GEAE as a replacement for Ni-based single crystal superalloys for use in high pressure turbine blades and vanes. The driving force for this research lies in the numerous property advantages offered by NiAl alloys (ref. 2) over their superalloy counterparts. These include a reduction of density by as much as a third without significantly sacrificing strength, higher melting point, greater thermal conductivity, better oxidation resistance, and a better response to thermal barrier coatings. The current drawback to high strength NiAl single crystals is their limited ductility. Consequently, significant efforts including the work agreement with GEAE are underway to develop testing and design methodologies for these materials.

The approach to validation and component analysis involves the following steps (Fig. 2): determination of the statistical nature and source of fracture in a high strength, NiAl single crystal turbine blade material; measurement of the failure strength envelope of the material; coding of statistically based reliability models; verification of the code and model; and modeling of turbine blades and vanes for rig testing.

Material Testing and Specimen Design

Brittle materials frequently fail from a single, strength limiting origin due to low toughness. The strength of such a system is thus governed by the weakest-link within the system and is therefore dependent on the surface area and volume stressed during testing. Weibull statistics (ref. 5) are commonly used for reliability analysis of components fabricated from such materials. The calculated failure probability is dependent on the stress state and the material properties of the component.

Several isotropic theories applicable to ceramics and glasses have been incorporated into the public domain CARES (ref. 1) code developed at NASA Lewis. This post-processor code, when combined with a finite element stress analysis, calculates fast fracture probability of a brittle, monolithic structural component. As part of the cooperative agreement with GEAE the code will be modified to model anisotropic materials, such as single crystal NiAl.

The material being considered has limited ductility, is highly anisotropic (Young's modulus varies 95 to 271 GPa; 13.78 E3 ksi to 39.305 E3 ksi) and made in relatively small billets (25 x 50 x 100 mm; 0.98 x 1.96 x 3.94 in.) that will be used individually to produce a vane or blade. Therefore, the statistical nature and

[1] Resident research associate at NASA LeRC.

source of fracture is being studied via flexural testing of beam specimens (ref. 3), with statistical analysis of the data and fractography performed on all of the post-tested samples (ref. 4). Flexural testing allows many samples to be removed from a particular region of a given billet, thereby allowing determination of billet-to-billet and within billet consistency. These factors will cause a variation in component reliability. Furthermore, in contrast to tensile testing, flexural testing allows the location of failure to be readily identified because the asymmetry of flexural loading results in a specific fracture pattern.

Two basic types of flaws are typically encountered in brittle materials such as ceramics or glasses: surface defects and volumetric defects. Volumetric defects include large grains, pores, agglomerates and inclusions, while surface defects include exposed volume defects (e.g. a pore machined open) and machining or handling damage that occurs during specimen/component fabrication (ref. 4).

Flexural strength results for the single crystal NiAl indicate the material to exhibit a wide dispersion in strength (Fig. 3) that can be characterized via normal or Weibull statistics. Failure origins were identified in 27 of 29 specimens tested. In all cases failure originated from regions of interdendritic precipitation (Fig. 4). These interdendritic regions always contained a Ni-Al-Hf rich phase (Fig. 5) that was confirmed by x-ray analysis to be the Heusler phase Ni_2AlHf. Roughly half of the initiation sites also contained HfC dendrites within the interdendritic Heusler phase (Fig 6). The HfC phase was identified by Auger electron spectroscopy and confirmed by the shape of the carbon peak (Fig. 7).

Other strength tests planned for verification work include flexure (3 and 4-point), pure tension, pure compression, torsion and biaxial flexure. To date, uniaxial and biaxial flexural tests (Fig. 3) have been conducted, and a torsion specimen is being designed and verified relative to handbook solutions. Verification of a failure theory can be accomplished via measurement of points on the failure envelope and comparison to predictions by the model and code (Fig. 8). Each point on the failure envelope represents a stress state and thus can be measured experimentally for a given material via strength testing with various geometries. As the material exhibits elastic anisotropy and variation in fracture toughness with orientation (ref. 7), several orientations will be considered in strength testing.

For the torsion specimen design, in an effort to conserve time, materials and machining costs, finite element analysis was used to characterize the stress response of several specimens. A baseline model and several variations were analyzed using the ANSYS 5.0 finite element package. The intent was to optimize the stress response of the specimen such that highest stresses would occur in the gage section of the specimen, thus concentrating failure within this section. Upon completion of the stress analysis, a CARES analysis was conducted for each specimen as well.

Each model consisted of three parts: the specimen, a three jaw chuck assembly used to grip the specimen, and a sleeve of surface elements around the volume of the specimen (see Fig. 9). Note that only half of the length of the specimen was modeled to take advantage of symmetry. A desired maximum principal stress of 800 MPa (116.0 ksi) was specified for each specimen. To obtain this stress level, a tangential force in the circumferential direction was applied at third points to the extremities of the chuck assembly.

A total of nine specimen geometries were analyzed. The use of parametric design language within ANSYS facilitated easy manipulation of design variables and model creation. The transition length between the gage section and the grip section of the specimen served as one design parameter. The gage diameter was the other. The different values for these parameters appear in Fig. 10. The intent was to eliminate stress risers in the transition section of the specimen and keep the maximum stress within the gage section. A constant, low stress field was also desirable in the grip section of the specimen. The baseline design satisfied both of these requirements. A plot of the first principal stress for this model is shown in Fig. 11. As the gage section of the specimen became larger, higher stresses began to migrate into the transition section and beyond into the grip section. Also, as the transition length between the grip and gage sections was changed, higher stresses began to migrate into the transition section. Of the nine designs, no model behaved better than the baseline design.

The subsequent reliability analyses reinforced these results. Developing a specimen with high probability of failure in the gage section and low or no probability of failure in the transition and grip sections was the objective. Since it is anticipated that this material will exhibit the so called "size effect" (i.e., decreasing component strength with increasing component size), the overall stressed area of the component would likely affect the reliability results. This factor was monitored as the results of the different models were compared. Again, the various iterations in the design provided no reason to switch from the baseline specimen design.

Component Analysis

As a starting point for the component feasibility study, a two dimensional finite element model of a double tang blade post and disk assembly was obtained from General Electric (see Fig. 12). This was used with the NiAl failure data (Fig. 3) to perform the reliability analysis. Fig. 13 shows the approach used for this type of analysis. Using this approach, the design engineer can concentrate on areas of the component which possess low reliability and modify them accordingly, thus leading to the optimization of the component.

Only the blade dove tail section was considered in the reliability analysis. Two separate analyses were conducted. The first used the entire set of 29 failure data points to calculate the Weibull parameters. The second involved the assumption that through improved processing techniques, the lowest five failure points would be eliminated, hence the Weibull parameters were calculated from the 24 highest failure strength values. The results of the reliability analysis and the respective Weibull parameters appear in Fig. 14. This analysis clearly shows the effect that reduced scatter has on a reliability of a component fabricated from a brittle material system.

This effort was successful in demonstrating the feasibility of such design procedures; however, to fully characterize a component fabricated from this type of material system, a failure criterion has to be developed that captures the anisotropic behavior of the material. This is a subject for future work and is identified as a milestone within the work agreement. Other areas of future work include a more complete characterization of the material's behavior along various crystallographic orientations. Billet to billet strength variation as well as strength variation within each billet will also be monitored.

References

1. N. Nemeth, J. Manderscheid, J. Gyekenyesi, "CARES Users and Programmers Manual," NASA Technical Paper TP2916, 1990.

2. Darolia, R., "NiAl For Turbine Airfoil Applications," in Structural Intermetallics, ed. R. Darolia et al., TMS, Warrendale, PA, 1993, pp. 495-504.

3. ASTM C 1161-90 "Standard Test Method for Flexural Strength of Advanced Ceramics at Ambient Temperature," American Society for Testing and Materials Annual Book of Standards, Vol. 15.01, 1990, pp. 333-339.

4. "Fractography and Characterization of Fracture Origins in Advanced Structural Ceramics," MIL-HDBK-790, (July, 1992).

5. W. Weibull, "A Statistical Theory of the Strength of Materials," Ingeniors Vetenskaps Akademien Handlinger, No. 151, 1939.

6. K. Chang, R, Darolia and H. Lipsitt, "Cleavage Fracture in B2 Aluminides," *Acta Metall.* Vol. 40, No. 10, 1992, pp. 2727-2737.

OBJECTIVE

- Modify and validate the CARES reliability code for use in design of components made from low ductility NiAl based intermetallics.

- This effort is part of a co–operative work agreement between General Electric Aircraft Engines and NASA LeRC.

Fig. 1 CD-94-66043

APPROACH

- Determine the statistical nature and source of fracture in high–strength NiAl single crystal material

- Measure the fracture strength envelope of the material (may involve characterizations in different material directions)

- Develop and code the appropriate failure model to capture both the statistical nature of failure and the anisotropic behavior of the material

- Verify the model and reliability code

- Model turbine vanes and blades for rig testing

Fig. 2 CD-94-66044

WEIBULL PLOT OF FAILURE DATA

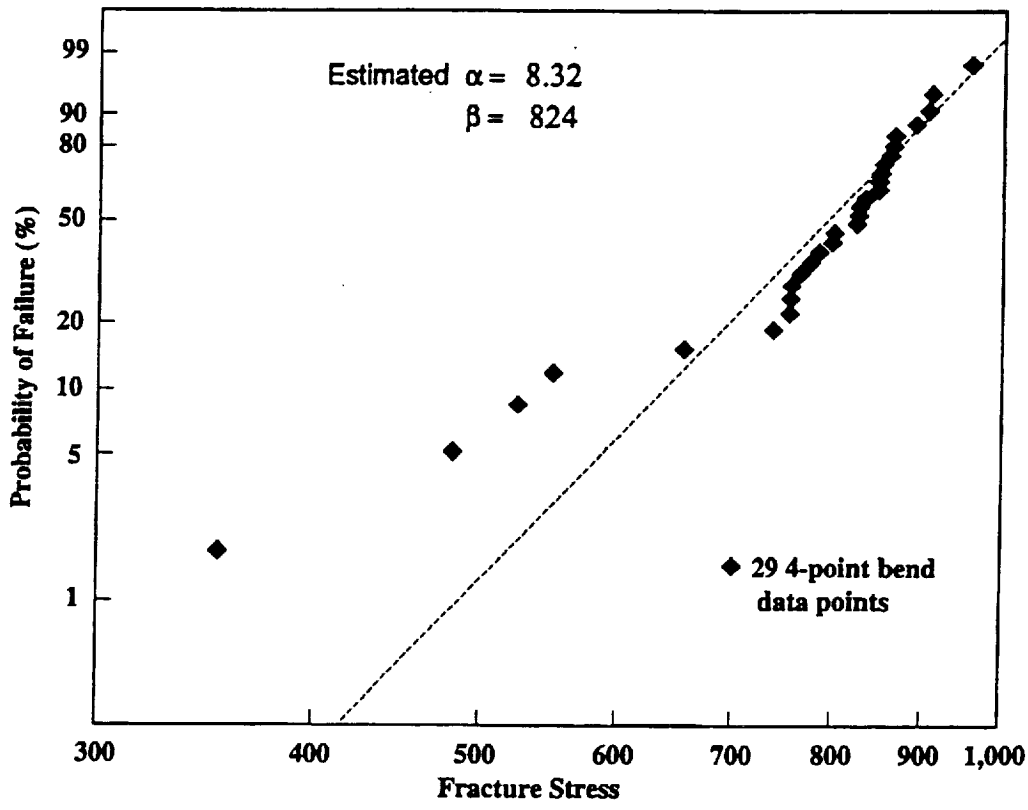

Fig. 3

CD-94-68045

NiAl TEST SPECIMEN FRACTOGRAPHY

— Fractography (SEM/EDS) was performed on 27 of 29 specimens (Origins for 2 were not recovered)

— All had fracture origins at Ni_2AlHf or HfC particles or a combined interdendritic particle

SEM image of failure origin

High mag. image of failure origin

Fig. 4

CD-94-68046

AUGER ANALYSIS SHOWING HEUSLER PHASE

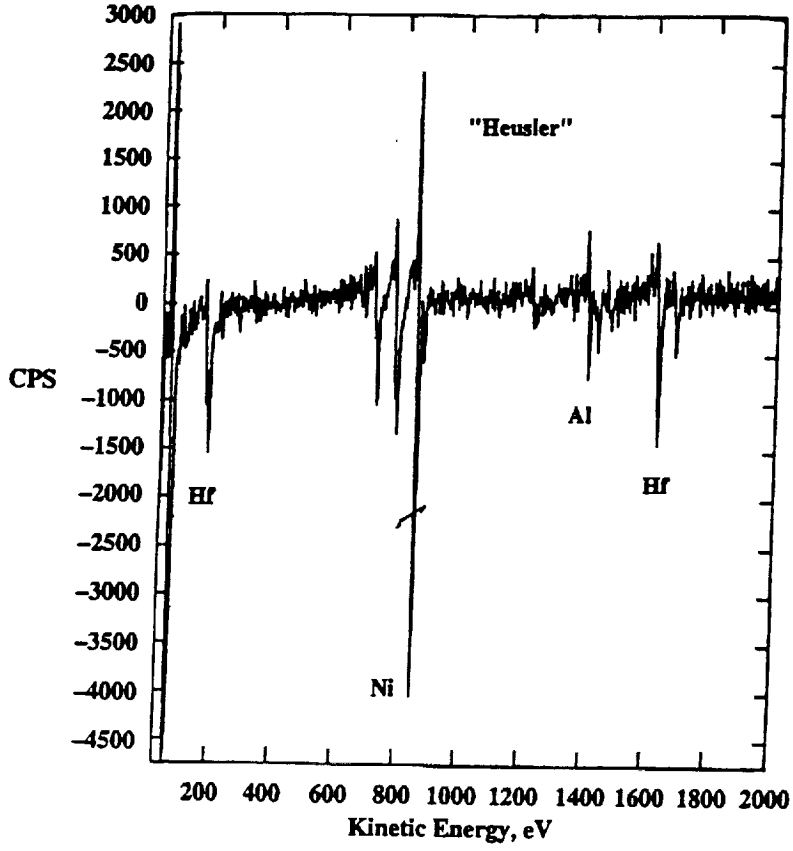

Fig. 5

CD-84-68047

AUGER ANALYSIS SHOWING HfC PHASE

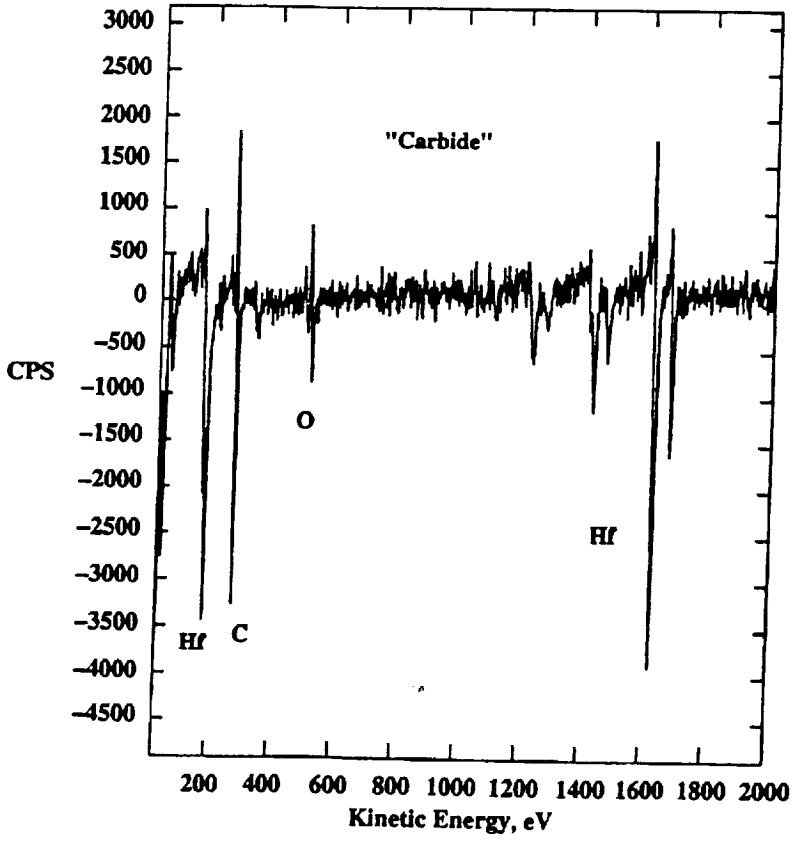

Fig. 6

CD-84-68048

DETAILED AUGER ANALYSIS OF CARBON REGION

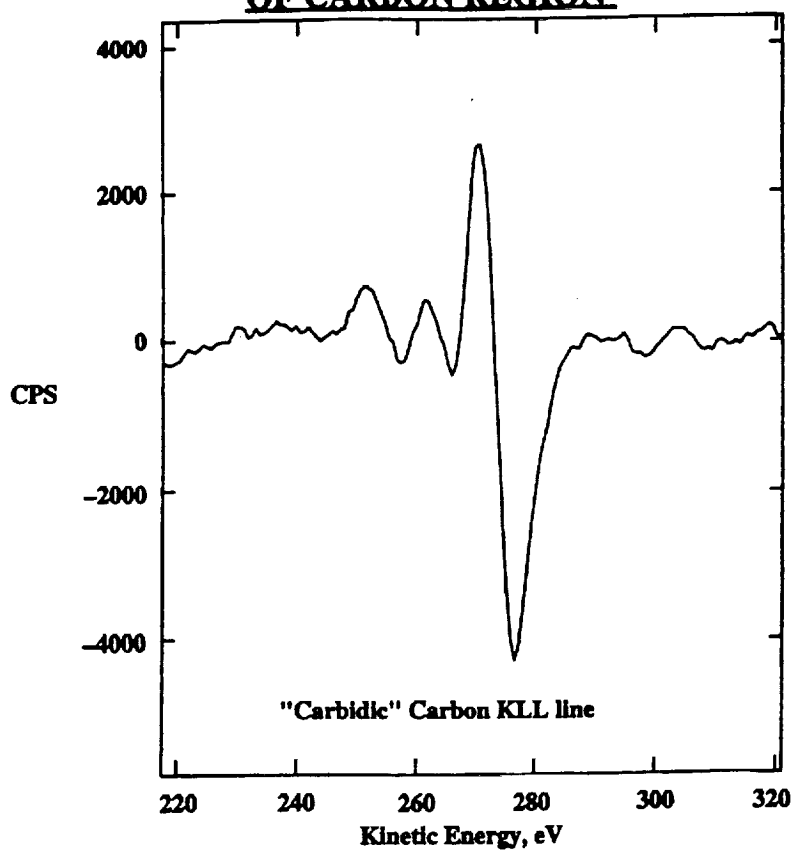

Fig. 7

CD-84-68048

COMPARISON OF FAILURE DATA WITH THEORY

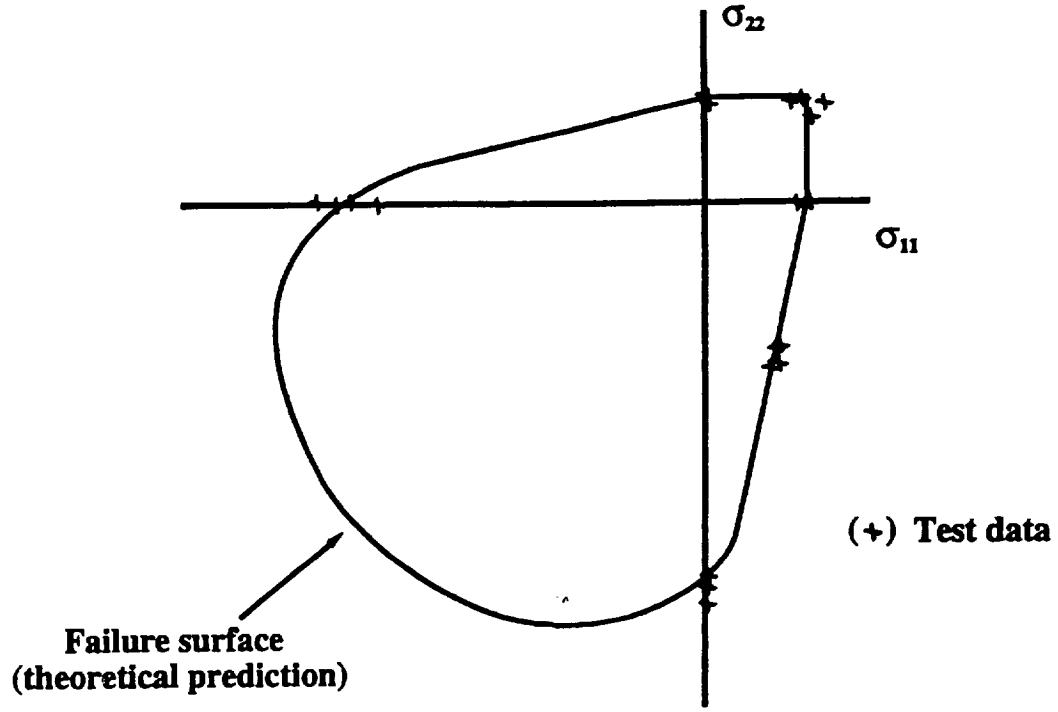

Fig. 8

CD-84-68050

TEST SPECIMEN ANALYSIS

Finite element model of specimen and chucks

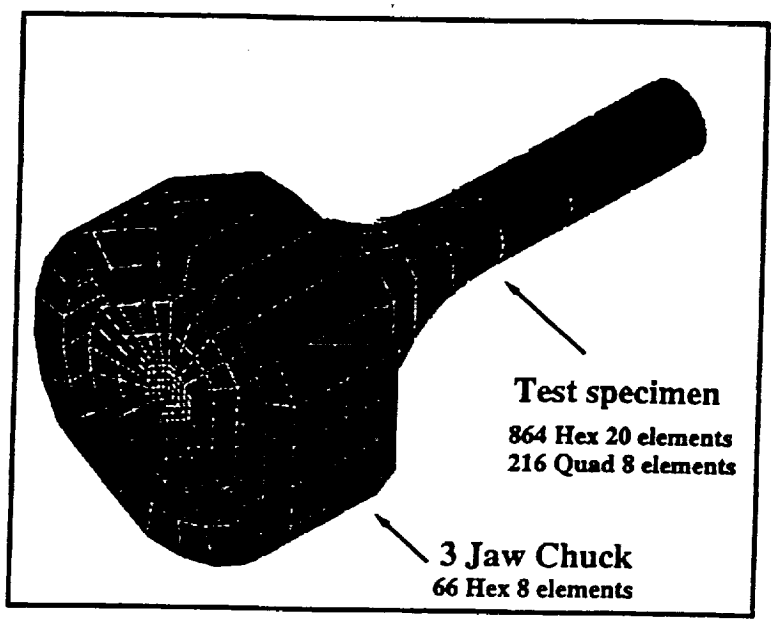

Fig. 9

CD-94-68051

TEST SPECIMEN
(BASE DESIGN)

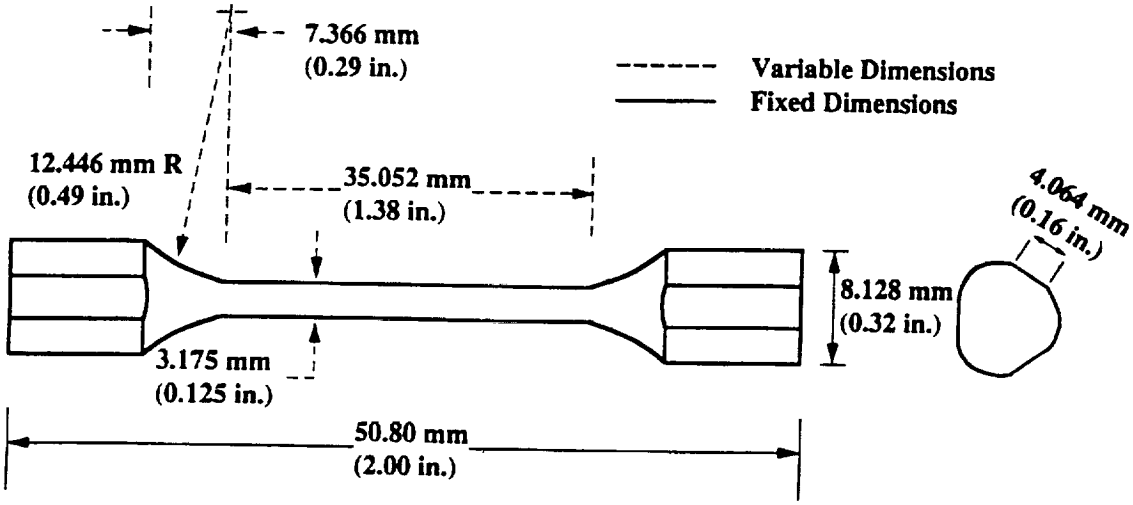

Gage Diameters:	3.175 mm	3.810 mm	4.445 mm
	(0.125 in.)	(0.150 in.)	(0.175 in.)
Transition lengths:	7.366 mm	5.004 mm	3.505 mm
	(0.29 in.)	(0.197 in.)	(0.138 in.)

Fig. 10

CD-94-68052

PRINCIPAL STRESS PLOT OF BASELINE TORSION SPECIMEN

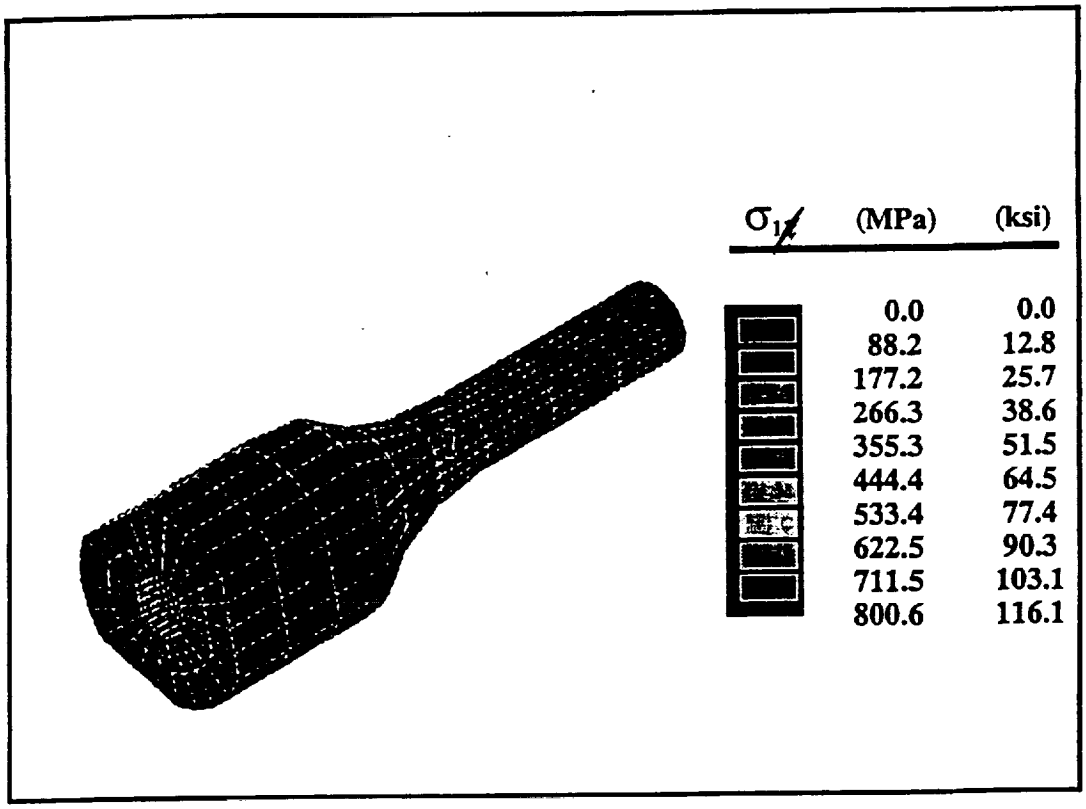

Fig. 11

CD-94-68053

PROBABILISTIC COMPONENT DESIGN PROCEDURE

- Approach:

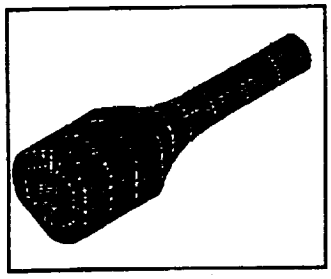

Test Specimen

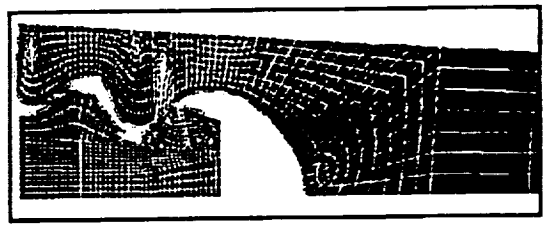

Complex Geometries

——→ Material failure characterization

——→ Fractographic examination of ruptured specimens

——→ Component finite-element analysis

——→ Component reliability evaluation

——→ Design optimization

Fig. 12

CD-94-68054

BLADE AND DISK ANALYSIS

Finite element model of blade post and disk assembly

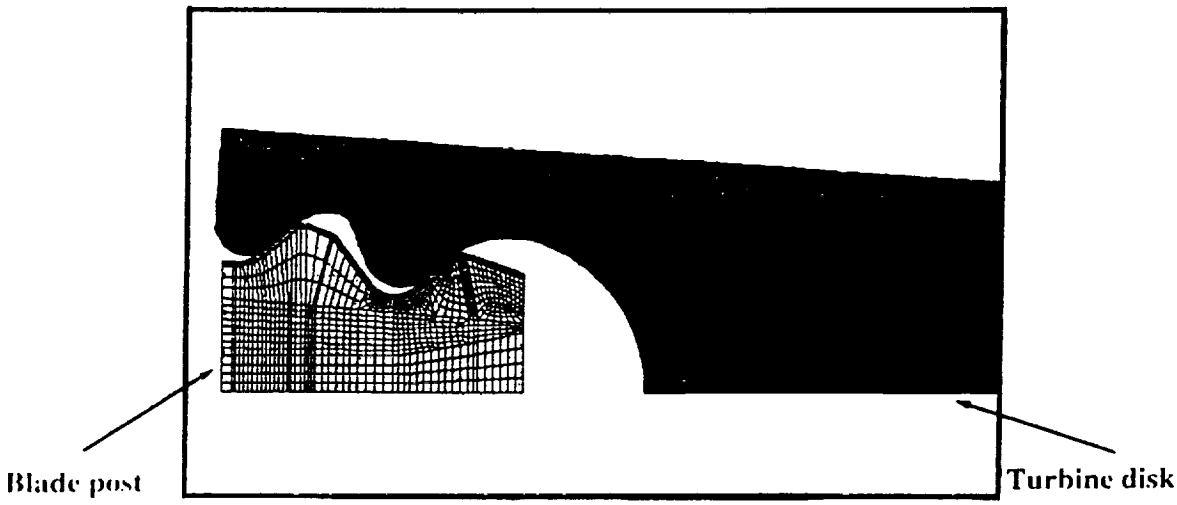

Fig. 13 CD-94-68056

SUMMARY OF CARES ANALYSIS OF BLADE

Two reliability analyses were conducted on blade design

– Two sets of Weibull parameters were used

	29 Data points	24 Data points
Alpha	**8.32**	**15.30**
Beta $(ksi)^{3/\alpha}$	**51,021**	**74,092**
Reliability	**99.46%**	**99.99%**

Fig. 14 CD-94-68056

CONCLUSIONS

- Failure origins can be identified in low ductility NiAl's with appropriate testing
- Torsion specimen geometry was verified through FEM and CARES analyses
- Methods in place for component reliability analyses
- Improved processing techniques can be used to improve component reliability

Fig. 15 CD-94-68057

FUTURE WORK

- Test material for billet to billet strength variation
- Test material for strength variation within a billet
- Test for statistical variation along different material directions
- Develop appropriate failure model for this material

Fig. 16 CD-94-68058

Design with Brittle Materials

ASM Handbook, Volume 20
Materials Selection and Design

Article 6-J

Stephen F. Duffy, PhD, PE
Cleveland State University
Cleveland, OH 44115
Phone: (216) 687-3874
Fax: (216) 687-9280

Lesley A. Janosik
NASA Lewis Research Center
21000 Brookpark Road, M.S. 6-1
Cleveland, OH 44135
Phone: (216) 433-5160
Fax: (216) 433-8300
E-Mail: Lesley.Janosik@lerc.nasa.gov

Design with Brittle Materials

1. Introduction

There is an increasing use of certain types of brittle materials (e.g., ceramics, intermetallics, and graphites) in the fabrication of lightweight components. From a design engineer's perspective, brittle materials often exhibit attractive high strength properties at service temperatures that are well beyond use temperatures of conventional ductile materials. For advanced diesel and turbine engines, ceramic components have already demonstrated functional abilities at temperatures reaching 1371 °C, which is well beyond the operational limits of most conventional metal alloys. However, a penalty is paid in that these materials typically exhibit low fracture toughness, which is usually defined by a critical stress intensity factor, and typically quantified by K_{IC}. This inherent undesirable property must be considered when designing components. Lack of ductility (i.e., lack of fracture toughness) leads to low strain tolerance and large variations in observed fracture strength. When a load is applied, the absence of significant plastic deformation or micro-cracking causes large stress concentrations to occur at microscopic flaws. These flaws are unavoidably present as a result of fabrication or in-service environmental factors. Note that non-destructive evaluation (NDE) inspection programs can not be successfully implemented during fabrication. The combination of high strength and low fracture toughness leads to relatively small critical defect sizes that can not be detected by current NDE methods. As a result, components with a distribution of defects (characterized by various sizes and orientations) are produced which leads to an observed scatter in component strength. Catastrophic crack growth for brittle materials occurs when the crack driving force or energy release rate reaches a critical value and the resulting component failure proceeds in a catastrophic manner.

The emphasis in this chapter is placed on design methodologies and characterization of certain material properties. Of particular interest to the design engineer is the inherent scatter in strength noted above. Accounting for this phenomenon requires a change in philosophy on the design engineer's part that leads to a reduced focus on the use of safety factors in favor of reliability analyses. If a brittle material with an obvious scatter in tensile strength is selected for its high strength attributes, or inert behavior, then components should be designed using an appropriate design

methodology rooted in statistical analysis. However, the reliability approach presented in this chapter demands that the design engineer must tolerate a finite risk of unacceptable performance. This risk of unacceptable performance is identified as a component's probability of failure (or alternatively, component reliability). The primary concern of the engineer is minimizing this risk in an economical manner.

This chapter will present fundamental concepts and models associated with performing time-independent and time-dependent reliability analyses for brittle materials exhibiting scatter in ultimate strength. However, the discussion contained within this chapter is not limited to materials exposed to elevated service temperatures. The concepts can be easily extended to more mundane applications where brittle materials such as glass or cements are utilized. Specific applications that have utilized ceramic materials at near ambient temperatures include wear parts (nozzles, valves, seals, etc.), cutting tools, grinding wheels, bearings, coatings, electronics, and human prostheses. Other brittle materials, such as glass and graphite materials, have been used in the fabrication of infrared transmission windows, glass skyscraper panels, television cathode ray tubes (CRTs), and high-temperature graphite bearings. Thus in this chapter the design methodologies used to analyze these types of components, as well as components exposed to elevated service temperatures, are presented. Reliability algorithms are outlined, and several applications are presented to further illustrate the utilization of these reliability algorithms in structural applications. For further background material on statistical methods, the reader is directed to see article 2-C.

2 Time-independent Reliability Analyses

An engineer is trained to quantify component failure through the use of a safety factor. By definition, the safety factor for a component subjected to a single load L is given by the ratio

$$Safety\ Factor = \frac{R}{L} \qquad \textbf{(Eq 1)}$$

where R is the resistance (or strength) of the material from which the component is fabricated. Making use of the concept of a safety factor, the probability of failure (P_f) for the component where a single load is applied is given by the expression

$$P_f = Probability\left(\frac{R}{L} \geq 1\right) \quad \textbf{(Eq 2)}$$

In making the transition from a deterministic safety factor for a component to a probability of failure, for the most general case, the assumption is made that both R and L are random variables. Under this assumption P_f is the product of two finite probabilities summed over all possible outcomes. Both probabilities are associated with an event and a random variable.

The first event is defined by the random variable L taking on a value in the range

$$\left(x - \frac{dx}{2}\right) \leq L \leq \left(x + \frac{dx}{2}\right) \quad \textbf{(Eq 3)}$$

The probability associated with this event is the area under the probability density function (PDF) for the load random variable (f_L) over this interval, i.e.,

$$P_1 = f_L(x)\,dx \quad \textbf{(Eq 4)}$$

The second event is associated with the probability that the random variable R is less than or equal to x. This is the area under the probability density for the resistance random variable (f_R) from minus infinity (or an appropriate lower limit defined by the range of the resistance random variable) to x. This second probability is given by the cumulative distribution function (CDF) for the resistance random variable (F_R) evaluated at x, i.e.,

$$P_2 = F_R(x) \quad \textbf{(Eq 5)}$$

With the probability of failure defined as the product of these two probabilities, summed over all possible values of x, then

$$\begin{aligned} P_f &= P_1 P_2 \\ &= \int_{-\infty}^{+\infty} F_R(x)\, f_L(x)dx \end{aligned} \quad \textbf{(Eq 6)}$$

To interpret this integral expression, consider the graphs in Fig 1. In this figure, the graph of an arbitrary probability density function for the resistance random variable is superimposed on the graph of an arbitrary probability density function for the load random variable. Note that R and L must have the same dimensional units (e.g., force or stress) to superimpose their graphs in the same figure. A common misconception is that P_f is the area of overlap

encompassed by the two probability density functions. Scrutiny of Eq 6 leads to the appropriate conclusion that the probability of failure is really the area under the composite function

$$g_{RL}(x) = F_R(x)\, f_L(x) \qquad \textbf{(Eq 7)}$$

which is also illustrated in Fig 1.

Next, consider the situation where the load random variable has very little scatter relative to the resistance random variable. For example, if a number of test specimens were fabricated from a brittle material, say for instance a monolithic ceramic, the ultimate tensile strength can easily vary by over 100%. That is, the highest strength value in the group tested can easily be twice as large as the lowest value. Variations of this magnitude are not typical for the load design variable, and the engineer could easily conclude that load is a deterministic design variable while strength is a random design variable. This assumption can be accommodated in this development by allowing the probability density function for the load random variable to be defined by the expression

$$f_L(x) = \delta(x - x_o) \qquad \textbf{(Eq 8)}$$

Here δ is the Dirac delta function defined as

$$\delta(x - x_o) = \begin{cases} \infty & x = x_o \\ 0 & x \neq x_o \end{cases} \qquad \textbf{(Eq 9)}$$

Note that the Dirac delta function satisfies the definition for a probability density function, i.e., the area under the curve is equal to one, and the function is greater than or equal to zero for all values of x. The Dirac delta function represents the scenario where the standard deviation of a random variable approaches zero in the limit, and the random variable takes on a single value, i.e., the central value identified here as x_o. Since the Dirac delta function is being used to represent the load random variable, then x_o really represents the deterministic magnitude of the applied load. Keep in mind that the applied load can have units of force or stress. However, load and resistance are commonly represented with units of stress. Thus x_o is replaced with σ, an applied stress, and the probability of failure is given by the expression

$$P_f = \int_{-\infty}^{+\infty} F_R(x)\delta(x - \sigma)dx \qquad \textbf{(Eq 10)}$$

However, with the Dirac delta function embedded in the integral expression, the probability of failure simplifies to

$$P_f = F_R(\sigma) \qquad \textbf{(Eq 11)}$$

Thus the probability of failure is equal to the CDF of the resistance random variable evaluated at the applied load, σ. The use of the Dirac delta function in representing the load design variable provides justification for the use of the Weibull CDF (or a similarly skewed distribution) in quantifying the probability of failure for components fabricated from ceramics or glass.

2.1 System Reliability

A unique property of most brittle materials is an apparent decrease in tensile strength as the size of the component increases. This is the so called size effect. As an example consider a simple component such as a uniaxial tensile specimen. Now suppose that two groups of these simple components have been fabricated. Each group is identical with the exception that the size of the specimens in the first group is uniformly smaller than the specimens in the second group. The mean sample strength from the first group would be consistently and distinctly larger in a manner that can not be accounted for by randomness. Thus Eq 11 must be transformed in some fashion to admit a size dependence. This is accomplished through the use of system reliability concepts. (See article 2-D for details on formulating the basic equations for system reliability.) After the following discussion the reader should be cognizant that the expression given in Eq 11 represents the probability of failure for a specified set of boundary conditions. If the boundary conditions are modified in any fashion, Eq 11 is no longer valid. To account for size effects and deal with the probability of failure for a component in a general manner, the component should be treated as a system, and the focus must be directed on the probability of failure of the system.

The typical approach to designing structural components with varying stress fields involves discretizing the component in order to characterize the stress field using finite element methods. Since component failure may initiate in any of the discrete elements, it is convenient to consider a component as a system and utilize system reliability theories. A component is a series system if it fails when one discrete element fails. This type of failure can be modeled using weakest-link reliability theories. A component is a parallel system when failure of a single element does not cause the component to fail. In this case the remaining elements sustain load through

redistribution. This type of failure can be modeled with what has been referred to in the literature as "bundle theories." Weakest-link theories and bundle theories represent represent the extremes of failure behavior modeled by reliability analysis. They suggest more complex systems such as "r out of n" systems. Here a component (system) of n elements functions if at least r elements have not failed. This type of system model has not found widespread application in structural reliability analysis. The assumption in this chapter is that the failure behavior of the brittle materials is sudden and catastrophic. This type of behavior fits within the description of a series system, thus a weakest-link reliability system is adopted.

Now the probability of failure of a discrete element must be related to the overall probability of failure of the component. If the failure of an individual element is considered a statistical event, and if these events are independent, then the probability of failure of a discretized component that acts as a series system is given by the expression

$$P_f = 1 - \prod_{i=1}^{N} (1 - \mathcal{P}_i) \qquad \text{(Eq 12)}$$

where N is the number of finite elements for a given component analysis. Here $\mathcal{P}_i$ is the probability of failure of the i^{th} discrete element.

In the next section an expression is specified for the probability of failure (or alternatively, the reliability) of the i^{th} discrete element for a simplified state of stress, i.e., a uniaxial tensile stress. The reader will also find that this expression allows the introduction of size scaling. Once size scaling relationships are established for a simple state of stress, the relationships are extended to multiaxial states of stress.

2.2 Two Parameter Weibull Distribution and Size Effects

In the ceramic and glass industry the Weibull distribution is universally accepted as the distribution of choice in representing the underlying probability distribution function for tensile strength. A two-parameter formulation and a three-parameter formulation are available for the Weibull distribution. However, the two-parameter formulation usually leads to a more conservative estimate for the component probability of failure. The two-parameter Weibull probability density function for a continuous random strength variable, denoted as Σ, is given by the expression

$$f_\Sigma(\sigma) = \left(\frac{\alpha}{\beta}\right)\left(\frac{\sigma}{\beta}\right)^{(\alpha-1)} \exp\left[-\left(\frac{\sigma}{\beta}\right)^{\alpha}\right] \qquad \textbf{(Eq 13)}$$

for $\sigma > 0$, and

$$f_\Sigma(\sigma) = 0 \qquad \textbf{(Eq 14)}$$

for $\sigma \leq 0$. The cumulative distribution is given by the expression

$$F_\Sigma(\sigma) = 1 - \exp\left[-\left(\frac{\sigma}{\beta}\right)^{\alpha}\right] \qquad \textbf{(Eq 15)}$$

for $\sigma > 0$, and

$$F_\Sigma(\sigma) = 0 \qquad \textbf{(Eq 16)}$$

for $\sigma \leq 0$. Here α (a scatter parameter, or Weibull modulus) and β (a central location parameter, or typically refered to as the Weibull scale parameter) are distribution parameters that define the Weibull distribution in much the same way as the mean (a central location parameter) and standard deviation (a scatter parameter) are parameters that define the Gaussian (normal) distribution. Note that in the ceramics and glass literature when the two-parameter Weibull formulation is adopted then "m" is used for the Weibull modulus α, and either σ_0 or σ_θ (see the discussion in the parameter estimation section regarding the difference between σ_0 and σ_θ) is used for the Weibull scale parameter. In this chapter the (α, β) notation is used exclusively and reference is made to the typical notation adopted in the ceramics literature. The reason for this is the tendency to overuse the "σ" symbol (e.g., σ_θ σ_0, σ_f-failure observation, and σ_t-threshold stress, etc.). Throughout this discussion the symbol "σ" will imply applied stress.

If the random variable representing uniaxial tensile strength of an advanced ceramic is characterized by a two-parameter Weibull distribution, i.e., the random strength parameter is governed by Eq 13 and Eq 14, then the probability that a uniaxial test specimen fabricated from an advanced ceramic will fail can be expressed by the cumulative distribution function

$$P_f = 1 - \exp\left[-\left(\frac{\sigma_{max}}{\beta_\theta}\right)^{\alpha}\right] \qquad \textbf{(Eq 17)}$$

Note that σ_{max} is the maximum normal stress in the component. When used in the context of characterizing the strength of ceramics and glasses, the central location parameter is referred to as the Weibull characteristic strength (β_0). In the ceramic literature this parameter can either be identified as the Weibull characteristic strength or the Weibull scale parameter. Since tensile strength is the random variable of interest, this parameter will be refered to as a strength parameter throughout the rest of this chapter. The characteristic strength is dependent on the uniaxial test specimen (tensile, flexural, pressurized ring, etc.) used to generate the failure data. For a given material, this parameter will change in magnitude with specimen geometry (the so-called size effect alluded to earlier). The Weibull characteristic strength typically has units of stress. The scatter parameter α is dimensionless.

With the tensile strength characterized by the two parameter Weibull distribution the discussion returns to the weakest link expression for component probability of failure defined by Eq 12. Let $\Re_i$ represent the reliability of the i^{th} continuum element where

$$\Re_i = 1 - \mathcal{P}_i \qquad \textbf{(Eq 18)}$$

The reliability of this continuum element is then governed by the following expression

$$\Re_i = exp\left(- \left(\frac{\sigma}{\beta_0} \right)^{\alpha} \Delta V \right) \qquad \textbf{(Eq 19)}$$

where σ is the principal tensile stress applied to the continuum element. The volume of this arbitrary continuum element is identified by ΔV. In this expression β_0 is the Weibull material scale parameter and can be described as the Weibull characteristic strength of a specimen with unit volume loaded in uniform uniaxial tension. This is a material specific parameter that is utilized in the component reliability analyses that follow. The dimensions of this parameter are stress·(volume)$^{1/\alpha}$.

The requisite size scaling discussed earlier is introduced by Eq 19. To demonstrate this, take the natural logarithm of Eq 19 twice, i.e.,

$$ln\, ln\left(\Re_i\right) = ln\left(- \left(\frac{\sigma}{\beta_0} \right)^{\alpha} \Delta V \right) \qquad \textbf{(Eq 20)}$$

Manipulation of Eq 20 yields

$$ln(\Delta V) = -\alpha ln(\sigma) + ln\, ln(\Re_i) + \alpha ln(-\beta_0) \quad \textbf{(Eq 21)}$$

With

$$y = ln(\Delta V) \quad \textbf{(Eq 22)}$$

$$x = ln(\sigma) \quad \textbf{(Eq 23)}$$

$$m = -\alpha \quad \textbf{(Eq 24)}$$

and

$$b = ln\, ln(\Re_i) + \alpha ln(-\beta_0) \quad \textbf{(Eq 25)}$$

then it is apparent that Eq 21 has the form of a straight line, i.e., $y = mx + b$.

Once again consider the two groups of test specimens fabricated from the same material mentioned earlier at the beginning of the section concerning system reliability. Recall that the specimens in each group are identical with each other, but the two groups have different gage sections such that ΔV (which is now identified as the gage section volume) is different for each group. Estimate Weibull parameters α and β_0 from the failure data obtained from either group (parameter estimation is discussed in detail in a following section). After the Weibull parameters are estimated the straight line in Fig 3 is located by setting $\Re_i$ equal to 0.5 (i.e., the 50th percentile) in Eq 21. This value for $\Re_i$ should establish a line that correlates well with the median values in each group.

Now return to the data sets mentioned above and establish the stress value associated with the median in each group. Plot the gage volumes (ΔV) of each group as a function of the median stress values in Fig 2. If no size effect is present the median failure strengths of the groups will fall close to a horizontal line. This would indicate no correlation between gage volume and the median strength value. Keep in mind that the discussion here could proceed using any percentile value, not just the 50th percentile. A systematic variation away from a horizontal line indicates indicates a size effect exists which must be considered in engineering design. If the median values for each group follows the trend indicated by the solid line in Fig 2 the design engineer should have no apprehensions using Weibull analysis with size scaling. Fig 1 and Fig 3 in Johnson and Tucker (Ref 1) are two excellent examples of these types of graphs with actual data.

The ability to account for size effects of individual elements was introduced through the expression for $\Re_i$ given by Eq 19. A rational approach for justifying this expression was outlined above. Now a general expression for the probability of failure for a component (i.e., a general form for Eq 17) is derived based on Eq 19. Under the assumptions that the component consists of an infinite number of elements (i.e., the continuum assumption) and that the component is best represented by a series system, then

$$P_f = 1 - \lim_{k\to\infty} \left(\prod_{i=1}^{k} \Re_i \right) \qquad \text{(Eq 26)}$$

Substituting for $\Re_i$ yields

$$P_f = 1 - exp\left(-\lim_{k\to\infty} \sum_{i=1}^{k} \left(\left(\frac{\sigma}{\beta_0} \right)^{\alpha} \Delta V \right)_i \right) \qquad \text{(Eq 27)}$$

Here ΔV once again represents the volume of an element. The limit inside the bracket is a Riemann sum. Thus

$$P_f = 1 - exp\left[-\int \left(\frac{\sigma}{\beta_0} \right)^{\alpha} dV \right] \qquad \text{(Eq 28)}$$

Weibull (Ref 2) first proposed this integral representation for the probability of failure. The expression is integrated over all tensile regions of the specimen volume if the strength-controlling flaws are randomly distributed through the volume of the material, or over all tensile regions of the specimen area if flaws are restricted to the specimen surface. For failures due to surface defects the probability of failure is given by the expression

$$P_f = 1 - exp\left[-\int \left(\frac{\sigma}{\beta_0} \right)^{\alpha} dA \right] \qquad \text{(Eq 29)}$$

which is derived in a manner similar to Eq 28.

The segregation of defect populations into volume and surface distributed flaws hints at the possibility of multiple defect populations. Johnson (Ref 3) presented an in depth treatment of this topic as it relates to ceramic materials. The Weibull material scale parameter β_0 has units of stress·(volume $)^{1/\alpha}$. If the strength controlling flaws are restricted to the surface of the specimens in a sample, then the Weibull material scale parameter has units of stress·(area $)^{1/\alpha}$. For a given specimen geometry, Eqs 17 and 28 can be equated, yielding an expression relating

β_0 and β_θ. Methods for converting β_θ to an equivalent β_0 value are addressed in ASTM Standard Practice C 1239-95.

2.3 Three Parameter Weibull Distribution

The three-parameter Weibull probability density function for a continuous random strength variable, denoted as Σ, is given by the expression

$$f_\Sigma(\sigma) = \left(\frac{\alpha}{\beta}\right)\left(\frac{\sigma-\gamma}{\beta}\right)^{(\alpha-1)} \exp\left[-\left(\frac{\sigma-\gamma}{\beta}\right)^{\alpha}\right] \qquad \textbf{(Eq 30)}$$

for $\sigma > \gamma$, and

$$f_\Sigma(\sigma) = 0 \qquad \textbf{(Eq 31)}$$

for $\sigma \leq \gamma$. In Eq 30 α is once again the Weibull modulus (or the shape parameter), β is the Weibull scale parameter, and γ is a threshold parameter. The cumulative distribution is given by the expression

$$F_\Sigma(\sigma) = 1 - \exp\left[-\left(\frac{\sigma-\gamma}{\beta}\right)^{\alpha}\right] \qquad \textbf{(Eq 32)}$$

for $\sigma > \gamma$, and

$$F_\Sigma(\sigma) = 0 \qquad \textbf{(Eq 33)}$$

for $\sigma \leq \gamma$. The same reasoning presented in the previous section on size scaling utilizing a two parameter formulation can be applied using the three parameter formulation. The resulting expression for the probability of failure of a component subjected to a single applied stress σ is

$$P_f = 1 - \exp\left[-\int\left(\frac{\sigma-\gamma}{\beta_0}\right)^{\alpha} dV\right] \qquad \textbf{(Eq 34)}$$

if the defect population is spatially distributed throughout the volume. A similar expression exists for failures due to area defects. The focus of the discussion in the next section turns to accommodating multiaxial stress states in Eq 28 and Eq 34. This involves the development of multiaxial reliability models.

The approach outlined in this section and previous sections to account for the scatter in failure strength and the size effect of brittle materials was first introduced by Weibull (Ref 2 and Ref 4). The concepts were based on the principles of weakest-link theory presented earlier. A number of authors including Pierce (Ref 5), Kontorova (Ref 6), as well as Frenkel and Kontorova (Ref 7) have made contributions in this area. In fact Pierce first proposed the weakest link concept while modeling yarn failure. However, Pierce assumed a Gaussian distribution for the strength random variable of yarn, and Weibull developed the unique probability density function for his work that now bears his name. Hu (Ref 8) explored the difficulties associated with parameter estimation when a Guassian or log normal distribution is adopted for the strength random variable. Shih (Ref 9) has shown that the three-parameter Weibull distribution is a more accurate approximation of brittle material behavior (specifically monolithic ceramics) than the Gaussian or other distributions. However, most analyses incorporate a two-parameter Weibull probability density function where the threshold stress (the value of applied stress below which the failure probability is zero) is taken as zero. The reliability predictions obtained using the two-parameter function are more conservative than those obtained with the three-parameter model.

2.4 Multiaxial Reliability Models

Over the years a number of reliability models have been presented that extend the uniaxial format of Eq 28 and Eq 34 to multiaxial states of stress. Only models associated with isotropic brittle materials are presented here. Anisotropic reliability models are beyond the scope of this chapter. The reader can consult the work of Duffy and co-workers (Ref 10 and Ref 11) for information pertaining to reliability models for brittle composites. The monolithic models highlighted here include the principle of independent action (PIA) model, the normal stress averaging (NSA) model, and Batdorf's model. A brief discussion is presented for each. A detailed development is omitted for the sake of brevity. In order to simplify the presentation of each model recast Eq 28 as

$$P_f = 1 - \exp\left[-\int \psi \, dV\right] \qquad \text{(Eq 35)}$$

where ψ is identified as a failure function per unit volume. What remains is the specification of the failure function ψ for each reliability model.

2.4.1 NSA and PIA - Phenomenological Models

To predict the time-independent (also referred to as fast-fracture) material response under multiaxial stress states Weibull (Ref 2) proposed calculating a failure function per unit volume (Weibull identified the function as the risk of rupture) by averaging the tensile normal stress raised to an exponent in all directions over the area of a unit radius sphere for volume flaws. This is known as the normal stress averaging (NSA) model where

$$\psi = k \bar{\sigma}_n^{\alpha} \qquad \textbf{(Eq 36)}$$

where

$$\bar{\sigma}_n^{\alpha} = \frac{\int_A \sigma_n^{\alpha} dA}{\int_A dA} \qquad \textbf{(Eq 37)}$$

and

$$k = \frac{(2\alpha + 1)}{(\beta_0)^{\alpha}} \qquad \textbf{(Eq 38)}$$

The area integration in Eq 37 is performed over the region of a unit sphere where σ_n (the Cauchy normal stress) is tensile. The reader is directed to the CARES Users and Programmers Manual (Ref 12) for a in depth explanation of the constants appearing in the equations above. Gross (Ref 13) demonstrated that for surface flaws this same averaging technique can be executed over the contour of a circle with a unit radius. Although the surface flaw technique is intuitively plausible for the NSA model, the approach is somewhat arbitrary. In addition, it lacks a closed-form solution, and therefore, requires computationally intensive numerical modeling.

Barnett et al. (Ref 14) and Freudenthal (Ref 15) proposed an alternative approach usually referred to as the principle of independent action (PIA) model. Here

$$\psi = \left(\frac{\sigma_1}{\beta_0}\right)^{\alpha} + \left(\frac{\sigma_2}{\beta_0}\right)^{\alpha} + \left(\frac{\sigma_3}{\beta_0}\right)^{\alpha} \qquad \textbf{(Eq 39)}$$

where σ_1, σ_2 and σ_3 are the three principal stresses at a given point. The PIA model is the probabilistic equivalent to the deterministic maximum stress failure theory.

The NSA model, and in particular the PIA model, have been widely applied in brittle material design. The reader is directed to works by Margetson (Ref 16), Paluszny and Wu (Ref 17), DeSalvo (Ref 18), Wertz, and Heitman (Ref 19), as well as Dukes (Ref 20) for a more in depth development and discussion of the merits of these two models. Historically, the NSA and the PIA models have been popular methods for multiaxial stress state analysis. However, the NSA and PIA models are in essence phenomenological and do not specify the nature of the defect causing failure. As a consequence, no foundation exists for extrapolating predictions made by these models to conditions different from the original test specimen configuration. Other models that are rooted in the principles of fracture mechanics will be discussed in the next section.

2.4.2. Batdorf's Theory - Mechanistic Model

The concepts proposed by Batdorf (Ref 21), and later refined by Batdorf and Crose (Ref 22), are important in that the approach incorporates a mechanistic basis for the effect of multiaxial states of stress into the weakest-link theory. Here material defects distributed throughout the volume (and/or over the surface) are assumed to have a random orientation. In addition, the defects are assume to be noninteracting discontinuities (cracks) with an assumed regular geometry. Failure is assumed to occur when a far field effective stress associated with the weakest flaw reaches a critical level. The effective stress is a predefined combination of the far field normal stress and the far field shear stress. It is also a function of the assumed crack configuration, the existing stress state, and the fracture criterion employed (hence the claim that the approach captures the physics of fracture). Accounting for the presence of a far-field shear stress reduces the far-field normal stress needed for fracture. This model is identified by taking

$$\psi = \alpha k_B \int_0^{(\sigma_e)_{max}} \frac{\Phi(\Sigma, \sigma_{cr})}{4\pi} \sigma_{cr}^{\alpha-1} \, d\sigma_{cr} \qquad \text{(Eq 40)}$$

where Φ is a solid angle that is dependent on the fracture criterion selected, the crack configuration and the applied stress state. The maximum effective stress $(\sigma_e)_{max}$ is defined as an equivalent mode I fracture stress for mixed mode loading. The crack density coefficient k_B is obtained from the following expression

$$k_B = \frac{\eta_v(\sigma_{cr})}{(\sigma_{cr})^a} \qquad \text{(Eq 41)}$$

Here σ_{Cr} is defined as the critical far field normal stress for a given crack configuration under mode I loading. Once again the reader is directed to the CARES Users and Programmers Manual (Ref 12) for a detailed interpretation of the parameters appearing in Eq 40. For the most part, the Batdorf model yields more accurate reliability analyses than those produced by either the NSA or PIA models.

Numerous authors have discussed the stress distribution around cavities of various types under different loading conditions, and proposed numerous criteria to describe impending fracture. Specifically investigators such as Giovan and Sines (Ref 23), Batdorf (Ref 21), Stout and Petrovic (Ref 24), as well as Petrovic and Stout (Ref 25) have compared results from the most widely accepted mixed-mode fracture criteria with each other and with selected experimental data. The semi-empirical equation developed by Palaniswamy and Knauss (Ref 26) and Shetty (Ref 27) seemingly provides enough flexibility to fit to experimental data. In addition, Shetty's criterion can account for the out-of-plane flaw growth that is observed under mixed-mode loadings. However, several issues must be noted. No prevailing consensus has emerged regarding a best probabilistic fracture theory. Most of the available criteria predict somewhat similar results, despite the divergence of initial assumptions. Moreover, one must approach the mechanistic models with some caution. The reliability models based on fracture mechanics incorporate the assumptions made in developing the fracture models on which they are based. One of the fundamental assumptions made in the derivation of fracture mechanics criteria is that the crack length is much larger than the characteristic length of the microstructure. This is sometimes referred to as the continuum principle in engineering mechanics. For the brittle materials discussed here that characteristic length is the grain size (or diameter). If one contemplates the fact that most brittle materials are high strength with an attending low fracture toughness, then the critical defect size can be quite small. If the critical defect size approaches the grain size of the material, then the phenomenological models discussed above may be more appropriate than the mechanistic models.

2.5 Parameter estimation

As indicated earlier, the distribution of choice for characterizing the tensile strength of brittle materials is the Weibull distribution. One fundamental reason for this choice goes beyond the fact that the Weibull distribution usually provides a good fit to the data. While the log-normal distribution often provides an adequate fit, it precludes any accounting of size effects. The reader is once again directed to work by Hu (Ref 8) for a detailed discussion on this matter. As it turns out, once a conscious choice is made to utilize the Weibull distribution, Eq 17 provides a convenient formulation for parameter estimation. However, one can not extract the fundamental distribution parameters needed for general component analysis from this expression, unless the test specimen has the same geometry and applied loads as the component. The fundamental distribution parameters (identified previously as material specific parameters) were embedded in Eq 28. Thus together, Eq 17 and Eq 28 provide a convenient method for extracting material specific parameters from failure data. The details are provided in the next section.

Tensile strength measurements are taken for one of two reasons: either for a comparison of the relative quality of two materials, or for the prediction of the failure probability for a structural component. The latter is the focus of this chapter, although the analytical details provided here allow for either. To obtain point estimates of the unknown Weibull distribution parameters, well-defined functions are utilized that incorporate the failure data and specimen geometry. These functions are referred to as estimators. It is desirable that an estimator be consistent and efficient. In addition, the estimator should produce unique, unbiased estimates of the distribution parameters. Different types of estimators exist, including: moment estimators, least-squares estimators, and maximum likelihood estimators. This discussion initially focuses on maximum likelihood estimators (MLE) due to the efficiency and the ease of application when censored failure populations are encountered. The likelihood estimators are used to compute parameters from failure populations characterized by a two-parameter Weibull distribution. Alternatively, non-linear regression estimators (discussed later) are utilized to calculate unknown distribution parameters for a three-parameter Weibull distribution.

Many factors affect the estimates of the distribution parameters. The total number of test specimens plays a significant role. Initially, the uncertainty associated with parameter estimates decreases significantly as the number of test specimens increases. However a point of diminishing returns occurs when the cost associated with performing

additional strength tests may not be justified by improvements in the estimated values of the distribution parameters. This suggests that a practical number of strength tests should be performed to obtain a desired level of confidence associated with a parameter estimate. This point can not be overemphasized. However, quite often 30 specimens (a widely cited rule-of-thumb) is deemed a sufficient quantity of test specimens when estimating Weibull parameters. One should immediately ask why 29 specimens would not suffice. Or more importantly, why is 30 specimens sufficient? The answer to this is addressed in ASTM Standard Practice C 1239-95 where the details of computing confidence bounds for the maximum likelihood estimates (these bounds are directly relate to the precision of the estimate) are presented. Duffy et al. (Ref 28) discusses the reasons why these same confidence bounds are not available for the non-linear regression estimators.

Tensile and flexural specimens are the most commonly used test configurations in determining ultimate strength values for brittle materials. However, as noted earlier, most brittle material systems exhibit a decreasing trend in material strength as the test specimen geometry is increased. Thus the observed strength values are dependent on specimen size and geometry. Parameter estimates can be computed based on a given specimen geometry; however, the parameter estimates should be transformed and utilized in a component reliability analysis as material-specific parameters. The procedure for transforming parameter estimates for the typical specimen geometries just cited is outlined in ASTM Standard Practice C 1239-95. The reader should be aware that the parameters estimated using non-linear regression estimators are material specific parameters. Therefore no transformation is necessary after these parameters have been estimated.

Brittle materials can easily contain two or more active flaw distributions (e.g., failures due to inclusions or machining damage) and each will have its own strength distribution parameters. The censoring techniques presented here for the two-parameter Weibull distribution require positive confirmation of multiple flaw distributions, which necessitates fractographic examination to characterize the fracture origin in each specimen. Multiple flaw distributions may also be indicated by a deviation from the linearity of the data from a single Weibull distribution (see Fig 3). However observations of approximately linear behavior should not be considered a sufficient reason to conclude a single flaw distribution is active. The reader is strongly encouraged to integrate mechanical failure data and fractographic analysis.

As was just noted, discrete fracture origins are quite often grouped by flaw distributions. The data for each flaw distribution can also be screened for outliers. An outlying observation is one that deviates significantly from other observations in the sample. However, an apparent outlying observation may be an extreme manifestation of the variability in strength. If this is the case, the data point should be retained and treated as any other observation in the failure sample. Yet the outlying observation can be the result of a gross deviation from prescribed experimental procedure, or possibly an error in calculating or recording the numerical value of the data point in question. When the experimentalist is clearly aware that either of these situations has occurred, the outlying observation may be discarded, unless the observation (i.e., the strength value) can be corrected in a rational manner. For the sake of brevity this discussion omits any discussion on the performance of fractographic analyses, and omits any discussion concerning outlier tests.

2.5.1 Two parameter Maximum Likelihood Estimators (MLE)

With the above discussion serving as background, attention is now focused on obtaining estimated values of the Weibull parameters α and β. This discussion focuses on maximum likelihood estimators (MLE) due to the efficiency, and the ease of application when censored failure populations are encountered. When a sample containing ultimate strength observations yields two or more distinct flaw distributions, the sample is said to contain censored data. The maximum likelihood methodology accounts for censored data in a rational, straight-forward manner. Other estimation techniques (specifically linear regression estimators) must appeal to ad hoc re-ranking schemes in the presence of censored data.

Johnson and Tucker (Ref 1), as well as others, have shown that the MLE method is more efficient in estimating parameters. Here efficiency is measured through the use of confidence bounds. For an equivalent confidence level these authors have demonstrated that the confidence bounds for a maximum likelihood estimate is always smaller than the confidence bound obtained using linear regression. For this reason the likelihood estimators should be used to compute parameters from failure populations characterized by a two parameter Weibull distribution.

The parameter estimates obtained using the maximum likelihood technique are unique (for a two-parameter Weibull distribution), and as the size of the sample increases, the estimates statistically approach the expected values of

the true population parameter. Let σ_1, σ_2, ... , σ_N represent realizations of the ultimate tensile strength (a random variable) in a given sample, where it is assumed that the ultimate tensile strength is characterized by the two-parameter Weibull distribution. The likelihood function associated with this sample is the joint probability density of the N random variables, and thus is a function of the unknown Weibull distribution parameters (α, β_θ). The likelihood function for an uncensored sample under these assumptions is given by the expression

$$L = \prod_{i=1}^{N} \left(\frac{\tilde{\alpha}}{\tilde{\beta}_\theta}\right)\left(\frac{\sigma_i}{\tilde{\beta}_\theta}\right)^{\tilde{\alpha}-1} exp\left[-\left(\frac{\sigma_i}{\tilde{\beta}_\theta}\right)^{\tilde{\alpha}}\right] \qquad \textbf{(Eq 42)}$$

The parameter estimates (the Weibull modulus $\tilde{\alpha}$ and the characteristic strength $\tilde{\beta}_\theta$) are determined by taking the partial derivatives of the logarithm of the likelihood function with respect to $\tilde{\alpha}$ and $\tilde{\beta}_\theta$, and equating the resulting expressions to zero. Note that the tildes will distinguish a parameter estimate from its corresponding true value. The system of equations obtained by differentiating the log likelihood function for a censored sample is given by

$$\frac{\sum_{i=1}^{N} (\sigma_i)^{\tilde{\alpha}} \ln(\sigma_i)}{\sum_{i=1}^{N} (\sigma_i)^{\tilde{\alpha}}} - \frac{1}{N}\sum_{i=1}^{N} \ln(\sigma_i) - \frac{1}{\tilde{\alpha}} = 0 \qquad \textbf{(Eq 43)}$$

and

$$\tilde{\beta}_\theta = \left[\left(\sum_{i=1}^{N} (\sigma_i)^{\tilde{\alpha}}\right)\frac{1}{N}\right]^{\frac{1}{\tilde{\alpha}}} \qquad \textbf{(Eq 44)}$$

Eq 43 is solved numerically, since a closed form solution for $\tilde{\alpha}$ can not be obtained from this expression. Once $\tilde{\alpha}$ is determined this value is inserted into Eq 44 and $\tilde{\beta}_\theta$ is calculated directly. The reader is once again directed to ASTM Standard Practice C 1239-95 for the expressions corresponding to samples with censored data.

2.5.2 Three Parameter Linear Regression

To date, most reliability analyses performed on structural components fabricated from ceramic materials have utilized the two-parameter form of the Weibull distribution. The use of a two-parameter Weibull distribution to characterize the random nature of material strength implies a non-zero probability of failure for the full range of applied

tensile stress. This represents a conservative design assumption when analyzing structural components. The three-parameter form of the Weibull distribution was presented earlier in Eqs 30 and 31. The additional parameter is a threshold stress (γ) that allows for zero probability of failure when the applied stress is at or below the threshold value. Certain monolithic ceramics have exhibited threshold behavior. The reader is directed to an extensive data base assembled by Quinn (Ref 29), the silicon nitride data in Foley et al. (Ref 30), as well as data (with supporting fractography) presented by Chao and Shetty (Ref 31) that was analyzed later in Duffy et al. (Ref 28).

When strength data indicates the existence of a threshold stress, a three-parameter Weibull distribution should be employed in the stochastic failure analysis of structural components. By employing the concept of a threshold stress, an engineer can effectively tailor the design of a component to optimize structural reliability. To illustrate the approach Duffy et al. (Ref 28) embedded the three-parameter Weibull distribution in a reliability model that utilized the principle of independent action (PIA). Analysis of a space shuttle main engine (SSME) turbo-pump blade predicted a substantial improvement in component reliability when the three-parameter Weibull distribution was utilized in place of the two-parameter Weibull distribution. Note that the three-parameter form of the Weibull distribution can easily be extended to Batdorf's (Ref 21 and Ref 22) model, reliability models proposed for ceramic composites by Duffy et al. (Ref 32), or Thomas and Wetherhold (Ref 33), as well as the interactive reliability models proposed by Palko (Ref 34).

The non-linear regression method presented here was first proposed by Margetson and Cooper (Ref 35). However, these estimators maintain certain disadvantages relative to bias and invariance, and these issues were explored numerically in Duffy et al. (Ref 28). The Monte Carlo simulations in Duffy et al. (Ref 28) demonstrated that the functions proposed by Margetson and Cooper (Ref 35) are neither invariant nor unbiased. However, they are asymptotically well behaved in that bias decreases and confidence intervals contract as the sample size increases. Thus, even though bias and confidence bounds may never be quantified using these non-linear regression technique, the user is guaranteed that estimated values improve as the sample size is increased.

Regression analysis postulates a relationship between two variables. In an experiment typically one variable can be controlled (the independent variable) while the response variable (or dependent variable) is not. In simple failure experiments the material dictates the strength at failure, indicating that the failure stress is the response variable.

The ranked probability of failure (P_i) can be controlled by the experimentalist, since it is functionally dependent on the sample size (N). After arranging the observed failure stresses ($\sigma_1, \sigma_2, \sigma_3, \cdots, \sigma_N$) in ascending order, and specifying

$$P_i = \frac{(i - 0.5)}{N} \qquad \textbf{(Eq 45)}$$

then clearly the ranked probability of failure for a given stress level can be influenced by increasing or decreasing the sample size. The procedure proposed by Margetson and Cooper (Ref 35) adopts this philosophy. They assume that the specimen failure stress is the dependent variable, and the associated ranked probability of failure becomes the independent variable.

Using the three-parameter version of Eq 34, an expression can be obtained relating the ranked probability of failure (P_i) to an estimate of the failure strength ($\tilde{\sigma}_i$). Assuming uniaxial stress conditions in a test specimen with a unit volume, Eq 34 yields

$$\tilde{\sigma}_i = \tilde{\gamma} + \tilde{\beta}_0 \left[ln\left(\frac{1}{1 - P_i}\right)\right]^{1/\tilde{\alpha}} \qquad \textbf{(Eq 46)}$$

where $\tilde{\alpha}$, β_0 and $\tilde{\gamma}$ are estimates of the shape parameter (α), the scale parameter (β_0), threshold parameter (γ), respectively. Expressions for the evaluation of these parameters for a test specimen subjected to pure bending are found in Duffy et al. (Ref 28). Defining the residual as

$$\delta_i = \tilde{\sigma}_i - \sigma_i \qquad \textbf{(Eq 47)}$$

where σ_i is the i^{th} ranked failure stress obtained from actual test data, then the sum of the squared residuals is expressed as

$$\sum_{i=1}^{N} (\delta_i)^2 = \sum_{i=1}^{N} \left[\tilde{\gamma} + \tilde{\beta}_0 \left(W_i\right)^{1/\tilde{\alpha}} - \sigma_i\right]^2 \qquad \textbf{(Eq 48)}$$

Here the notation of Margetson and Cooper (Ref 35) has been adopted where

$$W_i = ln\left(\frac{1}{1 - P_i}\right) \qquad \textbf{(Eq 49)}$$

Note that the forms of $\tilde{\sigma}_i$ and W_i change with specimen geometry. This is discussed in more detail in in Duffy et al. (Ref 28).

It should be apparent that the objective of this method is to obtain parameter estimates that minimize the sum of the squared residuals. Setting the partial derivatives of the sum of the squared residuals with respect to $\tilde{\alpha}$, β_0 and $\tilde{\gamma}$ equal to zero yields the following three expressions

$$\tilde{\beta}_0 = \frac{N\left[\sum_{i=1}^{N} \sigma_i (W_i)^{1/\tilde{\alpha}}\right] - \left[\sum_{i=1}^{N} \sigma_i\right]\left[\sum_{i=1}^{N} (W_i)^{1/\tilde{\alpha}}\right]}{N\sum_{i=1}^{N} (W_i)^{2/\tilde{\alpha}} - \left[\sum_{i=1}^{N} (W_i)^{1/\tilde{\alpha}}\right]\left[\sum_{i=1}^{N} (W_i)^{1/\tilde{\alpha}}\right]} \qquad \textbf{(Eq 50)}$$

$$\tilde{\gamma} = \frac{\left[\sum_{i=1}^{N} \sigma_i\right]\left[\sum_{i=1}^{N} (W_i)^{2/\tilde{\alpha}}\right] - \left[\sum_{i=1}^{N} \sigma_i (W_i)^{1/\tilde{\alpha}}\right]\left[\sum_{i=1}^{N} (W_i)^{1/\tilde{\alpha}}\right]}{N\sum_{i=1}^{N} (W_i)^{2/\tilde{\alpha}} - \left[\sum_{i=1}^{N} (W_i)^{1/\tilde{\alpha}}\right]\left[\sum_{i=1}^{N} (W_i)^{1/\tilde{\alpha}}\right]} \qquad \textbf{(Eq 51)}$$

and

$$\left| \sum_{i=1}^{N} \sigma_i (W_i)^{1/\tilde{\alpha}} \ln(W_i) - \tilde{\gamma} \sum_{i=1}^{N} \sigma_i (W_i)^{1/\tilde{\alpha}} \ln(W_i) - \tilde{\beta}_0 \sum_{i=1}^{N} \sigma_i (W_i)^{2/\tilde{\alpha}} \ln(W_i) \right| \leq \kappa_{conv} \qquad \textbf{(Eq 52)}$$

in terms of the parameter estimates. The solution of this system of equations is iterative, where the third expression is used to check convergence at iteration. The initial solution vector for this system is determined after assuming a convenient value for $\tilde{\alpha}$, say $\tilde{\alpha}$=1. Then β_0 is computed from Eq 50 and $\tilde{\gamma}$ is calculated from Eq 51. The values of these parameter estimates are then inserted into Eq 52 to determine if the convergence criterion is satisfied to within some predetermined tolerance (κ_{conv}). If this expression is not satisfied, $\tilde{\alpha}$ is updated and a new iteration is conducted. This procedure continues until a set of parameter estimates is determined that satisfy Eq 52.

The estimators perform reasonably well in comparison to estimates of the two-parameter Weibull distribution for the alumina data found in Table 1. Fig 4 is a plot of probability of failure versus failure stress for this data. The straight line represents the two-parameter fit to the data where $\tilde{\alpha}$= 143.2, β_0 = 395 ($\tilde{\gamma} \equiv 0$) using Quinn's (Ref 29) values for the shape and scale parameters. The non-linear curve represents the three-parameter fit to the data where $\tilde{\alpha}$ = 1.22, β_0 = 389, and $\tilde{\gamma}$ = 298. Note that the three-parameter distribution appears more efficient in predicting the failure data in the high reliability region of the graph. This is a qualitative assessment. Goodness-of-fit statistics such as the Kolmogorov-Smirnov statistic, the Anderson-Darling statistic, and likelihood ratio tests could provide quantitative measures to establish which form of the Weibull distribution would best fit the experimental data. These statistics are

utilized in conjunction with hypothesis testing to assess the significance level at which the null hypothesis can be rejected. Comparisons can then be made based on the value of the significance level.

2.6 Time-independent Reliability Algorithms

After a reliability model has been adopted and the failure function ψ has been specified, the primary task is the evaluation of the integral given in Eq 35. Closed form solutions exist for only the simplest of component geometries and boundary conditions. Therefore integrated computer algorithms have been developed that enable the design engineer to predict the time-independent (fast-fracture) reliability of components subjected to thermomechanical loading. Two algorithms are discussed here. One algorithm has been developed at the NASA Lewis Research Center and has been given the acronym CARES (Ceramics Analysis and Reliability Evaluation of Structures). This algorithm has been widely discussed in the literature by Nemeth et al. (Ref 12), Pai and Gyekenyesi (Ref 36), Gyekenyesi and Nemeth (Ref 37), as well as Gyekenyesi (Ref 38). The second computer algorithm was developed by AlliedSignal (Refs 39 and 40) with funding provided by the Department of Energy (DoE). Both algorithms are discussed briefly, and design examples are illustrated.

2.6.1 CARES Algorithm

The NASA Lewis Research Center CARES algorithm couples commercially available finite element programs, such as MSC/NASTRAN, ANSYS, or ABAQUS with the probabilistic design models discussed previously. The algorithm contains three software modules which: (1) perform parameter estimation utilizing experimental data obtained from standard laboratory specimens; (2) generate a neutral data base from MSC/NASTRAN, ABAQUS, and ANSYS finite element results files; and (3) evaluate the reliability of thermomechanically loaded components. Heat transfer and linear-elastic finite element analyses are used to determine the temperature field and stress field. The component reliability analysis module of CARES uses the thermoelastic or isothermal elastostatic results to calculate the time-independent reliability for each element utilizing a specified reliability model. Each element can be made arbitrarily small, such that the stress field in an element can be approximated as constant throughout the element (or subelement). The algorithm is compatible with most (but not all) two-dimensional elements, three-dimensional

elements, axisymmetric elements, and shell elements for the commercial finite element algorithms mentioned above. Reliability calculations are performed at the Gaussian integration points of the element or, optionally, at the element centroid. Using the element integration points enables the element to be divided into sub-elements, where integration point sub-volumes, sub-areas, and sub-temperatures are calculated. The location of the Gaussian integration point in the finite element and the corresponding weight functions are considered when the subelement volume and/or area is calculated. The number of subelements in each element depends on the integration order chosen, and the element type. If the probability of survival for each element is assumed to be a mutually exclusive event, the overall component reliability is the product of all the calculated element (or sub-element) survival probabilities. The CARES algorithm produces an optional PATRAN file containing risk-of-rupture intensities (a local measure of reliability) for graphical rendering of the structure's critical regions.

2.6.2 ERICA Algorithm

Unlike CARES, the AlliedSignal algorithm ERICA has a software architecture with a single module. Currently only one finite element program interface exists for the algorithm, i.e., an interface with the ANSYS finite element program. Once again stress and temperature information from the solution of a discretized component are used in conjunction with a specified reliability model to assess a component's reliability. ERICA admits multiple flaw distributions that can be spatially distributed through the volume, along the surface, and along the edges of a component. Both isotropic material behavior, and to a limited extent, anisotropic material behavior (for surface calculations) are taken into account. This anisotropic surface option allows the user to account for various types of surface finish on a component (e.g., ground, as fired, etc.). The ERICA algorithm can function on any platform that supports ANSYS. A limited number of element types are supported that offer the user some flexibility in modeling a component. Note that neither CARES nor ERICA support a full suite of elements for any of the commercial finite element algorithms.

2.7 Time-independent Design Examples

Reliability analyses are typically segregated into two categories: time-independent and time-dependent. This classification is rooted both in the historic development of the reliability models presented here and also in a practical approach to the analysis of a component. Yet in many instances, a component must perform in an adequate fashion over a pre-determined service life. To accomplish this design goal, the component must survive the initial load cycle. Thus the calculated time-independent reliability value is used as a screening criterion, and can also be used as an initial value for the time-dependent analyses discussed later. A fundamental premise of probabilistic analysis dictates that if the reliability of a component varies with time then it should never exceed the initial value (unless there exists some physical mechanism such as flaw healing that can account for this phenomenon). Typically materials deteriorate with time, and this assumption is incorporated throughout this chapter. From an historical perspective, the authors simply point out that the time-independent models were developed first (hence they are presented here first). In addition, the time-independent approach has been rigorously exercized over the years. Extensive design experience and data bases have been established prior to proposal of the time-dependent modeling efforts outlined later in this chapter.

Both the CARES and ERICA reliability algorithms have been utilized in the design and analysis of numerous structural components. Of the two, the NASA CARES algorithm has been more widely utilized for proprietary reasons. The CARES reliability algorithm has been used to design glass and ceramic parts for a wide range of applications. These include hot section components for turbine and internal combustion engines, bearings, laser windows on test rigs, radomes, radiant heater tubes, spacecraft activation valves and platforms, cathode ray tubes (CRTs), rocket launcher tubes, and ceramic packaging for microprocessors. Illustrated below are some typical design and analysis applications that have utilized the CARES software. In the interest of brevity, a complete example problem cannot be included in this article. For a complete step-by-step procedure on conducting a time-independent component reliability analysis, the reader is directed to the CARES Users and Programmers Manual (Ref 12).

The CARES algorithm has been successfully used in the development of ceramic turbocharger wheels (Ref 41). Specifically, the CARES algorithm was utilized to design the CTV7301 silicon nitride turbocharger rotor, depicted in Fig 5, which was implemented in the Caterpillar 3406E diesel engine. The reduced rotational inertia of the silicon nitride ceramic rotor compared to a metallic rotor significantly enhanced the turbocharger transient performance and

reduced emissions. Note that this was a joint effort involving AlliedSignal and Caterpillar and represents the first design and large-scale deployment of ceramic turbochargers in the United States. Over 1700 units have been supplied to Caterpillar Tractor Company for on-highway truck engines. These units together have accumulated a total of over 120 million miles of service.

Extensive work has been performed at the Fluid Systems Division of AlliedSignal Aerospace to analyze graphite and ceramic structural components such as high-temperature valves, test fixtures, and turbine wheels using CARES. A silicon nitride turbine wheel has been designed as a retrofit to replace components fabricated from waspalloy in a military cartridge-mode air turbine starter (Ref 42). The silicon nitride component reduced cost and weight while increasing resistance to temperature, erosion, and corrosion.

GTE Laboratories utilized the CARES algorithm in the analysis of a ceramic-to-metal brazed joint for automotive gas turbine engines (Ref 43 and Ref 44). A major design hurdle in ceramic-to-metal joining is the thermal expansion mismatch between the two different materials. This results in high residual stresses that increase the likelihood of ceramic failure. One of the goals of this work was to improve the capability of the metal shaft to transmit power by reducing concentrated tensile stresses. Their results confirmed the importance of probabilistic failure analysis for assessing the performance of various brazed joint designs.

A monolithic graphite spacecraft activation valve was designed by the Aerospace and Electronics Division of Boeing Space Defense Group (Ref 45). The valve directs reaction control gases for fine-tuning a high-performance kinetic energy kill vehicle's trajectory during the last 9 seconds of flight. Utilizing the CARES software, the valve was designed to withstand a gas pressure of 11.4 MPa (1.6 ksi) at 1930°C (3506 °F).

At the NASA-Lewis Research Center, a design study demonstrated the viability of an uncooled silicon nitride combustor for commercial application in a 300-kW engine with a turbine inlet temperature of 1370°C (2498 °F) (Ref 46). Using the CARES algorithm an analysis identified the most severe transient thermal stress in an emergency shutdown. The most critical area was found to be around the dilution port.

Ceramic poppet valves for spark ignition engines have been designed by TRW's Automotive Valve Division (Ref 47) as well as by General Motors. These parts depicted with other engine components in Fig 6 have been field tested in passenger cars, with excellent results. Potential advantages offered by these valves include reduced seat insert and

valve guide wear, improved valve train dynamics, increased engine output, and reduced friction loss using lower spring loads.

The largest known zinc-selenide (ZnSe) containment window (depicted in Fig 7) was been designed by Hughes Danbury Optical Systems (formerly Perkin-Elmer) utilizing the CARES algorithm. The window formed a pressure barrier between a cryogenic vacuum chamber containing optical equipment and a sensor chamber. The window measured 79 cm (31 inches) in diameter by 2.5 cm (1 inch) thick and was used in a test facility at Boeing for long-range infrared sensors.

The previous examples cited successful applications of the reliability algorithms in the design and analysis of commercial applications. In many instances the algorithms have been an integral component of research and development efforts in government supported programs. A specific example of this is the use of the CARES algorithm by participating organizations in the Advanced Turbine Technology Applications Program (ATTAP) to determine the reliability of structural component designs. The ATTAP program (Ref 48) is intended to advance the technological readiness of the ceramic automotive gas turbine engine. Structural ceramic components represent the greatest technical challenge facing the commercialization of such an engine, and are thus the prime project focus. Cooperative efforts have been developed between industry, key national facilities, and academia to capitalize on the unique capabilities and facilities developed for ceramic materials characterization and processing technology. Since the project's inception, Allison Engine Company has utilized the NASA-developed CARES software to design engine components, including structural, combustion, regeneration, and insulation applications all of which are depicted in Fig 8.

3. Life Prediction Using Reliability Analyses

The discussions in the previous sections assumed all failures were independent of time and history of previous thermomechanical loadings. However, as design protocols emerge for brittle material systems, designers must be aware of several innate characteristics exhibited by these materials. When subjected to elevated service temperatures, they exhibit complex thermomechanical behavior that is both inherently time-dependent and hereditary in the sense that current behavior depends not only on current conditions, but also on thermomechanical history. The design engineer

must also be cognizant that the ability of a component to sustain load degrades over time due to a variety of effects such as oxidation, creep, stress corrosion, and cyclic fatigue. Stress corrosion and cyclic fatigue result in a phenomenon called subcritical crack growth (SCG). This failure mechanism initiates at a pre-existing flaw and continues until a critical length is attained. At that point the crack grows in an unstable fashion leading to catastrophic failure. The SCG failure mechanism is a time-dependent load-induced phenomenon. Time-dependent crack growth can also be a function of chemical reaction, environment, debris wedging near the crack tip, and deterioration of bridging ligaments. Fracture mechanism maps, such as the one developed by Quinn (Ref 49) for ceramic materials depicted in Fig 9, help illustrate the relative contribution of various failure modes as a function of temperature and stress.

In addition to the Weibull shape and scale parameters discussed previously, analysis of time-dependent reliability in brittle materials necessitates accurate stress field information, as well as evaluation of distinct parameters reflecting material, microstructural, and/or environmental conditions. Predicted lifetime reliability of brittle material components depends on Weibull and fatigue parameters estimated from rupture data obtained from widely used tests involving flexural or tensile specimens. Fatigue parameter estimates are obtained from naturally flawed specimens ruptured under static, cyclic, or dynamic (constant stress rate) loading. For other specimen geometries, a finite element model of the specimen is also required when estimating these parameters. For a more detailed discussion of time-dependent parameter estimation, the reader is directed to the CARES/*Life* (CARES/Life Prediction Program) Users and Programmers Manual (Ref 50). This information can then be combined with stochastic modeling approaches and incorporated into integrated design algorithms (computer software) in a fashion similar to that presented previously for time-independent models. The theoretical concepts upon which these time-dependent algorithms have been constructed and the effects of time-dependent mechanisms, most notably subcritical crack growth and creep, will be addressed in the remaining sections of this chapter.

Although it will not be discussed in detail here, one approach to improve the confidence in component reliability predictions is to subject the component to proof testing prior to placing it in service. Ideally, the boundary conditions applied to a component under proof testing simulate those conditions the component would be subjected to in service, and the proof test loads are appropriately greater in magnitude over a fixed time interval. This form of testing eliminates the weakest components and, thus, truncates the tail of the strength distribution curve. After proof

testing, survived components can be placed in service with greater confidence in their integrity and a predictable minimum service life.

3.1 Need for Correct Stress State

With increasing use of brittle materials in high temperature structural applications, the need arises to accurately predict thermomechanical behavior. Most current analytical methods for both subcritical crack growth and creep models utilize elastic stress fields in predicting the time-dependent reliability response of components subjected to elevated service temperatures. Inelastic response at high temperature has been well documented in the materials science literature for these material systems, but this issue has been ignored by the engineering design community. However, the authors wish to emphasize that accurate predictions of time-dependent reliability demand accurate stress field information. From a design engineer's perspective, it is imperative that the inaccuracies of making time-dependent reliability predictions based on elastic stress fields are taken into consideration. The current section addresses this issue by presenting a recent formulation of a viscoplastic constitutive theory to model the inelastic deformation behavior of brittle materials at high temperatures.

Early work in the field of metal plasticity indicated that inelastic deformations are essentially unaffected by hydrostatic stress. This is not the case for brittle (e.g., ceramic-based) material systems, unless the material is fully dense. The theory presented here allows for fully dense material behavior as a limiting case. In addition, as Chuang and Duffy (Ref 51) point out, these materials exhibit different time-dependent behavior in tension and compression. Thus inelastic deformation models for these materials must be constructed in a fashion that admits sensitivity to hydrostatic stress and differing behavior in tension and compression.

A number of constitutive theories for materials that exhibit sensitivity to the hydrostatic component of stress have been proposed that characterize deformation using time-independent classical plasticity as a foundation. Corapcioglu and Uz (Ref 52) reviewed several of these theories by focusing on the proposed form of the individual yield function. The review includes the works of Kuhn and Downey (Ref 53), Shima and Oyane (Ref 54) and Green (Ref 55). Not included is the work by Gurson (Ref 56) who not only developed a yield criteria and flow rule, but also

discussed the role of void nucleation. Subsequent work by Mear and Hutchinson (Ref 57) extended Gurson's work to include kinematic hardening of the yield surfaces.

Although the previously mentioned theories admit a dependence on the hydrostatic component of stress, none of these theories allow different behavior in tension and compression. In addition, the aforementioned theories are somewhat lacking in that they are unable to capture creep, relaxation, and rate-sensitive phenomena exhibited by brittle materials at high temperature. Noted exceptions are the recent work by Ding et al. (Ref 58), as well as the work by White and Hazime (Ref 59). Another exception is an article by Liu et al. (Ref 60) which is an extension of the work presented by Ding and coworkers. As these authors point out, when subjected to elevated service temperatures, brittle materials exhibit complex thermo-mechanical behavior that is inherently time dependent, and hereditary in the sense that current behavior depends not only on current conditions, but also on thermo-mechanical history.

The macroscopic continuum theory formulated in the remainder of this section captures these time dependent phenomena by developing an extension of a J_2 plasticity model first proposed by Robinson (Ref 61) and later extended to sintered powder metals by Duffy (Ref 62). Although the viscoplastic model presented by Duffy (Ref 62) admitted a sensitivity to hydrostatic stress, it did not allow for different material behavior in tension and compression.

Willam and Warnke (Ref 63) proposed a yield criterion for concrete that admits a dependence on the hydrostatic component of stress and explicitly allows different material responses in tension and compression. Several formulations of their model exist, i.e., a three-parameter formulation and a five-parameter formulation. For simplicity, the overview of the multiaxial derivation of the viscoplastic constitutive model presented here builds on the three-parameter formulation. The attending geometrical implications have been presented elsewhere by Janosik and Duffy (Ref 64 and Ref 65). A quantitative assessment has yet to be conducted since the material constants have not been suitably characterized for a specific material . The quantitative assessment could easily dovetail with the nascent efforts of White and coworkers (Ref 59).

The complete theory is derivable from a scalar dissipative potential function identified here as Ω. Under isothermal conditions, this function is dependent upon the applied stress σ_{ij} and internal state variable α_{ij}

$$\Omega = \Omega\left(\sigma_{ij}, \alpha_{ij}\right) \qquad \textbf{Eq (53)}$$

The stress dependence for a J_2 plasticity model or a J_2 viscoplasticity model is usually stipulated in terms of the deviatoric components of the applied stress, $S_{ij}=\sigma_{ij}-(1/3)\sigma_{kk}\delta_{ij}$, and a deviatoric state variable, $\alpha_{ij}=\alpha_{ij}-(1/3)\alpha_{kk}\delta_{ij}$. For the viscoplasticity model presented here, these deviatoric tensors are incorporated along with the effective stress, $\eta_{ij}=\sigma_{ij}-\alpha_{ij}$, and an effective deviatoric stress, identified as $\Sigma_{ij}=S_{ij}-\alpha_{ij}$. Both tensors, i.e., η_{ij} and Σ_{ij}, are utilized for notational convenience.

The potential nature of Ω is exhibited by the manner in which the flow and evolutionary laws are derived. The flow law is derived from Ω by taking the partial derivative with respect to the applied stress

$$\dot{\varepsilon}_{ij} = \frac{\partial \Omega}{\partial \sigma_{ij}} \qquad \textbf{Eq (54)}$$

The adoption of a flow potential and the concept of normality, as expressed in Eq 54, were introduced by Rice (Ref 66). In his work the above relationship was established using thermodynamic arguments. The authors wish to point out that Eq 54 holds for each individual inelastic state.

The evolutionary law is similarly derived from the flow potential. The rate of change of the internal stress is expressed as

$$\dot{\alpha}_{ij} = -h \frac{\partial \Omega}{\partial \alpha_{ij}} \qquad \textbf{Eq (55)}$$

where h is a scalar function of the inelastic state variable (i.e., the internal stress) only. Using arguments similar to Rice's, Ponter and Leckie (Ref 67) have demonstrated the appropriateness of this type of evolutionary law.

To give the flow potential a specific form, the following integral format proposed by Robinson (Ref 61) is adopted

$$\Omega = K^2\left[\left(\frac{1}{2\mu}\right)\int F^n dF + \left(\frac{R}{H}\right)\int G^m dG\right] \qquad \textbf{Eq (56)}$$

where μ, R, H, and K are material constants. In this formulation μ is a viscosity constant, H is a hardening constant, n and m are unitless exponents, and R is associated with recovery. The octahedral threshold shear stress K appearing in Eq 56 is generally considered a scalar state variable which accounts for isotropic hardening (or softening). However, since isotropic hardening is often negligible at high homologous temperatures ($T/T_m \geq 0.5$), to a first

approximation K is taken to be a constant for metals. This assumption is adopted in the present work for brittle materials. The reader is directed to the work by Janosik (Ref 68) for specific details regarding the experimental test matrix needed to characterize these parameters.

The dependence upon the effective stress Σ_{ij} and the deviatoric internal stress a_{ij} are introduced through the scalar functions $F=F(\Sigma_{ij}, \eta_{ij})$ and $G=G(a_{ij}, \alpha_{ij})$. Inclusion of η_{ij} and α_{ij} will account for sensitivity to hydrostatic stress. The concept of a threshold function was introduced by Bingham (Ref 69) and later generalized by Hohenemser and Prager (Ref 70). Correspondingly, F will be referred to as a Bingham-Prager threshold function. Inelastic deformation occurs only for those stress states where $F(\Sigma_{ij}, \eta_{ij})>0$.

For frame indifference, the scalar functions F and G (and hence Ω) must be form invariant under all proper orthogonal transformations. This condition is ensured if the functions depend only on the principal invariants of Σ_{ij}, a_{ij}, η_{ij}, and α_{ij}; that is, $F=F(\tilde{I}_1, \tilde{J}_2, \tilde{J}_3)$, where $\tilde{I}_1=\eta_{ii}$, $\tilde{J}_2=(1/2)\Sigma_{ij}\Sigma_{ij}$, $\tilde{J}_3=(1/3)\Sigma_{ij}\Sigma_{jk}\Sigma_{ki}$ and $G=G(I_1, J_2, J_3)$, where $I_1=a_{ii}$, $J_2=(1/2)a_{ij}a_{ij}$, $J_3=(1/3)a_{ij}a_{jk}a_{ki}$. These scalar quantities are elements of what is known in invariant theory as an integrity basis for the functions F and G.

A three parameter flow criterion proposed by Willam and Warnke (Ref 63) will serve as the Bingham-Prager threshold function, F. The Willam-Warnke criterion uses the previously mentioned stress invariants to define the functional dependence on the Cauchy stress (σ_{ij}) and internal state variable (α_{ij}). In general, this flow criterion can be constructed from the following general polynomial

$$F = \lambda\left(\frac{\sqrt{\tilde{J}_2}}{\sigma_c}\right) + B\left(\frac{\tilde{I}_1}{\sigma_c}\right) - 1 \qquad \textbf{Eq (57)}$$

where σ_c is the uniaxial threshold flow stress in compression and B is a constant determined by considering homogeneously stressed elements in the virgin inelastic state $\alpha_{ij}=0$.

Note that a threshold flow stress is similar in nature to a yield stress in classical plasticity. In addition, λ is a function dependent on the invariant J_3 and other threshold stress parameters that are defined momentarily. The specific details in deriving the final form of the function F can be found in Willam and Warnke (Ref 63), and this final formulation is stated here as

$$F\left(\tilde{I}_1, \tilde{J}_2, \tilde{J}_3\right) = \frac{1}{\sigma_c}\left[\frac{1}{r(\tilde{\theta})}\right]\left[\frac{2\tilde{J}_2}{5}\right]^{1/2} + \frac{\tilde{I}_1}{3\rho\sigma_c} - 1 \qquad \textbf{Eq (58)}$$

for brevity. The invariant $\tilde{I}_1$ in Eq 70 admits a sensitivity to hydrostatic stress. The function F is implicitly dependent on J_3 through the function $r(\tilde{\theta})$, where the angle of similitude, $(\tilde{\theta})$, is defined by the expression

$$\cos\left(3\tilde{\theta}\right) = \frac{\left(3\sqrt{3}\right)\tilde{J}_3}{2\left(\tilde{J}_2\right)^{3/2}} \qquad \textbf{Eq (59)}$$

The invariant J_3 accounts for different behavior in tension and compression, since this invariant changes sign when the direction of a stress component is reversed. The parameter ρ characterizes the tensile hydrostatic threshold flow stress. For the Willam-Warnke three-parameter formulation, the model parameters include σ_t, the tensile uniaxial threshold stress, σ_c, the compressive uniaxial threshold stress, and σ_{bc}, the equal biaxial compressive threshold stress

A similar functional form is adopted for the scalar state function G. However, this formulation assumes a threshold does not exist for the scalar function G, and follows the framework of previously proposed constitutive models based on Robinson's (Ref 61) viscoplastic law.

Employing the chain rule for differentiation and evaluating the partial derivative of Ω with respect to σ_{ij}, and then with respect to α_{ij} as indicated in Eqs 54 and 55, yields the flow law and the evolutionary law, respectively. These expressions are dependent on the principal invariants (i.e., $\tilde{I}_1$, $\tilde{J}_2$, $\tilde{J}_3$, I_1, J_2,, and J_3,) the three Willam-Warnke threshold parameters (i.e., σ_t, σ_c, and σ_{bc}), and the flow potential parameters utilized in Eq 56 (i.e., R, H, K, and m). These expressions constitute a multiaxial statement of a constitutive theory for isotropic materials, and will serve as an inelastic deformation model for ceramic materials.

The overview presented in this section is intended to provide a qualitative assessment of the capabilities of this viscoplastic model in capturing the complex thermomechanical behavior exhibited by brittle materials at elevated service temperatures. Constitutive equations for the flow law (strain rate) and evolutionary law have been formulated based on a threshold function which exhibits a sensitivity to hydrostatic stress and allows different behavior in tension and compression. Further, inelastic deformation is treated as inherently time-dependent. A rate of inelastic strain is

associated with every state of stress. As a result, creep, stress relaxation, and rate sensitivity are phenomena resulting from applied boundary conditions and are not treated separately in an ad hoc fashion. Incorporating this model into a non-linear finite element code would provide a tool for the design engineer to numerically simulate the inherently time-dependent and hereditary phenomena exhibited by these materials in service.

3.2 Life Prediction Reliability Models

The ability of a brittle material component to sustain load degrades over time due to a variety of effects such as oxidation, creep, stress corrosion, and fatigue. Time-dependent probabilistic component design involves predicting the probability of failure for a thermomechanically loaded component based on specimen rupture data. Typically these experiments are performed using many simple geometry flexural or tensile test specimens. A static (creep), or dynamic (cyclic) load is applied to each specimen until fracture. Statistical strength and SCG (subcritical crack growth, or fatigue) parameters are then determined from these data. Using these statistical parameters, a time-dependent reliability model such as those discussed in the following section, and the results obtained from a finite element analysis, the life of a component with complex geometry and loading can be predicted. This life is interpreted as a component's reliability as a function of time. When the component reliability falls below a predetermined value, the associated point in time at which this occurs is assigned the life of the component. This design methodology presented herein combines the statistical nature of strength-controlling flaws with the mechanics of crack growth to allow for multiaxial stress states, concurrent (simultaneously occurring) flaw populations, and scaling effects. With this type of integrated design tool, a design engineer can make appropriate design changes until an acceptable time to failure has been reached. In the sections that follow only creep rupture and fatigue failure mechanisms are discussed. Although models that account for subcritical crack growth and creep rupture are presented, the reader is cautioned that currently available creep models for advanced ceramics have limited applicability due to the phenomenological nature of the models. There is a considerable need to develop models incorporating both the ceramic material behavior and microstructural events.

3.2.1 Subcritical Crack Growth

A wide variety of brittle materials, including ceramics and glasses, exhibit the phenomenon of delayed fracture or fatigue. Under the application of a loading function of magnitude smaller than that which induces short term failure, there is a regime where subcritical crack growth occurs and this can lead to eventual component failure in service. SCG is a complex process involving a combination of simultaneous and synergistic failure mechanisms. These can be grouped into two categories: (1) crack growth due to corrosion, and (2) crack growth due to mechanical effects arising from cyclic loading. Stress corrosion reflects a stress-dependent chemical interaction between the material and its environment. Water, for example, has a pronounced deleterious effect on the strength of glass and alumina. In addition, higher temperatures also tend to accelerate this process. Mechanically induced cyclic fatigue is dependent only on the number of load cycles and not on the duration of the cycle. This phenomenon can be caused by a variety of effects, such as debris wedging or the degradation of bridging ligaments, but essentially it is based on the accumulation of some type of irreversible damage that tends to enhance crack growth. Service environment, material composition, and material microstructure determine if a brittle material will display one, none, or some combination of these fatigue mechanisms.

Lifetime reliability analysis accounting for subcritical crack growth under cyclic and/or sustained loads is essential for the safe and efficient utilization of brittle materials in structural design. Because of the complex nature of SCG, models that have been developed tend to be semi-empirical and approximate the behavior of subcritical crack growth phenomenologically. Theoretical and experimental work in this area has demonstrated that lifetime failure characteristics can be described by consideration of the crack growth rate versus the stress intensity factor (or the range in the stress intensity factor). This is graphically depicted (see Fig. 10) as the logarithm of the rate of crack growth versus the logarithm of the mode I stress intensity factor. Curves of experimental data show three distinct regimes or regions of growth. The first region (denoted by I in Fig 10) indicates threshold behavior of the crack, where below a certain value of stress intensity the crack growth is zero. The second region (denoted by II in Fig 10) shows an approximately linear relationship of stable crack growth. The third region (denoted by III in Fig 10) indicates unstable crack growth as the materials critical stress intensity factor is approached. For the stress corrosion failure mechanism, these curves are material and environment sensitive. This model, using conventional fracture mechanics relationships,

satisfactorily describes the failure mechanisms in materials where at high temperatures, plastic deformations and creep behave in a linear visco-elastic manner (Ref 71). In general, at high temperatures and low levels of stress, failure is best described by creep rupture which generates new cracks (Ref 72). The creep rupture process will be discussed further in the next section.

The most often cited models in the literature regarding SCG are based on power law formulations. Other theories, most notably Wiederhorn's (Ref 73), have not achieved such widespread usage, although they may also have a reasonable physical foundation. Power law formulations are used to model both the stress corrosion phenomenon and the cyclic fatigue phenomenon. This modeling flexibility, coupled with their widespread acceptance, make these formulations the most attractive candidates to incorporate into a design methodology. A power law formulation is obtained by assuming the second crack growth region is linear and that it dominates over the other regions. Three power law formulations are useful for modeling brittle materials: the power law, the Paris law, and the Walker equation. The power law (Ref 71) (Ref 74) describes the crack velocity as a function of the stress intensity factor, and implies that the crack growth is due to stress corrosion. For cyclic fatigue, either the Paris law (Ref 75) or Walker's (Ref 76) (Ref 77) modified formulation of the Paris law is used to model the subcritical crack growth. The Paris law describes the crack growth per load cycle as a function of the range in the stress intensity factor. The Walker equation relates the crack growth per load cycle to both the range in the crack tip stress intensity factor and the maximum applied crack tip stress intensity factor. It is useful for predicting the effect of the R-ratio (the ratio of the minimum cyclic stress to the maximum cyclic stress) on the material strength degradation.

Expressions for time-dependent reliability are usually formulated based on the mode I equivalent stress distribution transformed to its equivalent stress distribution at time $t=0$. Investigations of mode I crack extension (Ref 78) have resulted in the following relationship for the equivalent mode I stress intensity factor

$$K_{Ieq}(\Psi,t) = \sigma_{Ieq}(\Psi,t)\ Y\ \sqrt{a(\Psi,t)} \qquad \text{(Eq 60)}$$

where $\sigma_{Ieq}(\Psi,t)$ is the equivalent mode I stress on the crack, Y is a function of crack geometry, $a(\Psi,t)$ is the appropriate crack length, and Ψ represents a spatial location within the body and the orientation of the crack. In some models such as the Weibull and PIA, Ψ represents a location only. Y is a function of crack geometry; however, herein it is assumed

constant with subcritical crack growth. Crack growth as a function of the equivalent mode I stress intensity factor is assumed to follow a power law relationship

$$\frac{da(\Psi,t)}{dt} = A\ K_{Ieq}^{N}(\Psi,t) \quad \text{(Eq 61)}$$

where A and N are material/environmental constants. The transformation of the equivalent stress distribution at the time of failure, $t=t_f$, to its critical effective stress distribution at time $t=0$ is expressed (Ref 79) (Ref 80)

$$\sigma_{Ieq,0}(\Psi,t_f) = \left[\frac{\int_0^{t_f} \sigma_{Ieq}^{N}(\Psi,t)\ dt}{B} + \sigma_{Ieq}^{N-2}(\Psi,t_f) \right]^{\frac{1}{(N-2)}} \quad \text{(Eq 62)}$$

where

$$B = \frac{2}{A\ Y^2\ K_{IC}^{N-2}\ (N-2)} \quad \text{(Eq 63)}$$

is a material/environmental fatigue parameter, K_{Ic} is the critical stress intensity factor, and $\sigma_{Ieq}(\Psi,t_f)$ is the equivalent stress distribution in the component at time $t=t_f$. The dimensionless fatigue parameter N is independent of fracture criterion. B is adjusted to satisfy the requirement that for a uniaxial stress state, all models produce the same probability of failure. The parameter B has units of stress^2 × time.

Because SCG operates on existing flaws in a material, the weakest-link statistical theories discussed previously are required to predict the time-dependent lifetime reliability for brittle materials. A subcritical crack growth model (e.g., the previously discussed power law, Paris law, or Walker equation) is combined with either the two- or three-parameter Weibull cumulative distribution function to characterize the component failure probability as a function of service lifetime. The effects of multiaxial stresses are considered by using the principle of independent action (PIA) model, the Weibull normal stress averaging (NSA) method, or the Batdorf theory. These multiaxial reliability expressions were outlined in the previous discussion on time-independent reliability analysis models, and, for brevity, will not be repeated here. The reader is directed to see the previous discussion or, for more complete details, to consult the CARES/*Life* Users and Programmers Manual (Ref 50).

3.2.2 Creep Rupture

For brittle materials the term creep can infer two different issues. The first relates to catastrophic failure of a component from a defect that has been nucleated and propagates to critical size. This is known as creep rupture to the design engineer. Here it is assumed that failure does not occur from a defect in the original flaw population. Unlike subcritical crack growth, which is assumed to begin at preexisting flaws in a component and continue until the crack reaches a critical length, creep rupture typically entails the nucleation, growth, and coalescence of voids which eventually form macrocracks which then propagate to failure. The second issue related to creep reflects back on subcritical crack growth as well as creep rupture, i.e., creep deformation. This section focuses on the former, while the latter (i.e., creep deformation) was discussed in a previous section.

Currently, most ceramic researchers utilize deterministic approaches to predict lifetime due to creep rupture. Stochastic methodologies for predicting creep life in ceramic components have not reached a level of maturity comparable to those developed for predicting fast-fracture and SCG reliability. One such theory is based on the premise that both creep and SCG failure modes act simultaneously (Ref 81). Another alternative method for characterizing creep rupture in ceramics was developed by Duffy and Gyekenyesi, (Ref 82), who developed a time-dependent reliability model that integrates continuum damage mechanics principles and Weibull analysis. This particular approach assumes that the failure processes for SCG and creep are distinct and separable activities.

The remainder of this section outlines this approach, highlighting creep rupture with the intent to provide the design engineer with a method to determine an allowable stress for a given component lifetime and reliability. This is accomplished by coupling Weibull theory with the principles of continuum damage mechanics, which was originally developed by Kachanov (Ref 83) to account for tertiary creep and creep fracture of ductile metal alloys.

Ideally, any theory that predicts the behavior of a material should incorporate parameters that are relevant to its microstructure (grain size, void spacing, etc.). However, this would require a determination of volume averaged effects of microstructural phenomena reflecting nucleation, growth, and coalescence of microdefects that in many instances interact. This approach is difficult even under strongly simplifying assumptions. In this respect, Leckie (Ref 84) points out that the difference between the materials scientist and the engineer is one of scale. He notes the materials scientist is interested in mechanisms of deformation and failure at the microstructural level and

the engineer focuses on these issues at the component level. Thus the former designs the material and the latter designs the component. Here, we adopt the engineer's viewpoint and note from the outset that continuum damage mechanics does not focus attention on microstructural events, yet this logical first approach does provide a practical model which macroscopically captures the changes induced by the evolution of voids and defects.

This method uses a continuum damage approach where a continuity function, ϕ, is coupled with Weibull theory to render a time-dependent damage model for ceramic materials. The continuity function is given by the expression

$$\phi = \left[1 - b(\sigma_0)^m \ (m+1)t\right]^{(1/(m+1))} \qquad \textbf{(Eq 64)}$$

where b and m are material constants, σ_0 is the applied uniaxial stress on a unit volume, and t is time. From this, an expression for a time to failure, t_f, can be obtained by noting that when $t = t_f$, $\phi = 0$. This results in the following

$$t_f = \frac{1}{b(\sigma_0)^m (m+1)} \qquad \textbf{(Eq 65)}$$

which leads to the simplification of ϕ as follows

$$\phi = \left[1 - (t / t_f)\right]^{(1/(m+1))} \qquad \textbf{(Eq 66)}$$

The above equations are then coupled with an expression for reliability to develop the time-dependent model. The expression for reliability for a uniaxial specimen is

$$R = exp\left[-V(\sigma / \beta)^{\alpha}\right] \qquad \textbf{(Eq 67)}$$

where V is the volume of the specimen, α is the Weibull shape parameter and β is the Weibull scale parameter. Incorporating the continuity function into the reliability equation, and assuming a unit volume yields

$$R = \exp\left[-(\sigma_0 / \phi\beta)^{\alpha}\right] \qquad \textbf{(Eq 68)}$$

Substituting for ϕ in terms of the time to failure results in the time-dependent expression for reliability

$$R = exp\left\{-\left(\frac{\sigma_0}{\beta}\right)^{\alpha}\left[1 - \frac{t}{t_f}\right]^{-\left(\frac{\alpha}{m+1}\right)}\right\} \qquad \textbf{(Eq 69)}$$

This model has been presented in a qualitative fashion, intending to provide the design engineer with a reliability theory that incorporates the expected lifetime of a brittle material component undergoing damage in the creep rupture regime. The predictive capability of this approach depends on how well the macroscopic state variable ϕ captures the growth of grain boundary microdefects. Finally, note that the kinetics of damage also depend significantly on the direction of the applied stress. In the above development, it was expedient from a theoretical and computational standpoint to use a scalar state variable for damage since only uniaxial loading conditions were considered. The incorporation of a continuum damage approach within a multiaxial Weibull analysis necessitates the description of oriented damage by a second-order tensor.

3.3 Life Prediction Reliability Algorithms

The computer programs CARES/*Life* (Ceramics Analysis and Reliability Evaluation of Structures/Life prediction program) and the AlliedSignal algorithm ERICA have the capability to evaluate the time-dependent reliability of monolithic ceramic components subjected to thermomechanical and/or proof test loading. The reader is directed to previously cited references (Ref 39 and Ref 40) for a detailed discussion of the life prediction capabilities of the ERICA algorithm. The CARES/*Life* program is an extension of the previously discussed CARES program, which predicted the fast-fracture (time-independent) reliability of monolithic ceramic components. CARES/*Life* retains all of the fast-fracture capabilities of the CARES program, and additionally includes the ability to perform time-dependent reliability analysis due to subcritical crack growth (SCG). CARES/*Life* accounts for the phenomenon of subcritical crack growth by utilizing the power law, Paris law, or Walker equation. The two-parameter Weibull cumulative distribution function is used to characterize the variation in component strength. The probabilistic nature of material strength and the effects of multiaxial stresses are modeled using either the principle of independent action (PIA), the Weibull normal stress averaging method (NSA), or the Batdorf theory. Parameter estimation routines are available for obtaining inert strength and fatigue parameters from rupture strength data of naturally flawed specimens loaded in static, dynamic, or cyclic fatigue. Fatigue parameters can be calculated using either the median value technique (Ref 85), a least squares regression technique, or a median deviation regression method which is somewhat similar to

trivariant regression (Ref 85). In addition, CARES/*Life* can predict the effect of proof testing on component service probability of failure. Creep and material healing mechanisms are not addressed in the CARES/*Life* code.

3.4 Life Prediction Design Examples

Once again, due to the proprietary nature of the ERICA algorithm, the life prediction examples presented in this section are all based on design applications where the NASA CARES/*Life* algorithm was utilized. Either algorithm should predict the same results cited here. However, at this point in time comparative studies utilizing both algorithms for the same analysis are not available in the open literature. The primary thrust behind CARES/*Life* is the support and development of advanced heat engines, and related ceramics technology infrastructure. DOE and Oak Ridge National Laboratory (ORNL) have several ongoing programs such as the Advanced Turbine Technology Applications Project (ATTAP) (Ref 86) (Ref 87) for automotive gas turbine development, the Heavy Duty Transport Program for low-heat-rejection heavy duty diesel engine development, and the Ceramic Stationary Gas Turbine (CSGT) program for electric power cogeneration. Both CARES/*Life* and the previously discussed CARES program are used in these projects to design stationary and rotating equipment, including turbine rotors, vanes, scrolls, combustors, insulating rings, and seals. These programs are also integrated with the DOE/ORNL Ceramic Technology Project (CTP) (Ref 88) characterization and life prediction efforts (Ref 89) (Ref 90).

Solar Turbines Incorporated is using CARES/*Life* to design hot-section turbine parts for the CSGT development program (Ref 91) sponsored by the DOE Office of Industrial Technology. This project seeks to replace metallic hot section parts with uncooled ceramic components in an existing design for a natural-gas-fired industrial turbine engine operating at a turbine rotor inlet temperature of 1120°C (2048°F). At least one stage of blades (Fig 11) and vanes, as well as the combustor liner, will be replaced with ceramic parts. Ultimately, demonstration of the technology will be proved with a 4000-hr engine field test.

Ceramic pistons for a constant-speed drive are being developed at Sundstrand Corporation's Aerospace Division. Constant-speed drives are used to convert variable engine speed to a constant output speed for aircraft electrical generators. The calculated probability of failure of the piston is less than 0.2×10^{-5} under the most severe limit-load condition. This program is sponsored by the U.S. Navy and ARPA (Advanced Research Projects Agency, formerly

DARPA - Defense Advanced Research Projects Agency). As depicted in Fig 12, Sundstrand has designed ceramic components for a number of other applications, most notably for aircraft auxiliary power units.

Glass components behave in a similar manner as ceramics and must be designed using reliability evaluation techniques. Using the CARES/*Life* software, Phillips Display Components Company has analyzed the possibility of alkali strontium silicate glass CRTs spontaneously imploding (Ref 92). CRTs are under a constant static load due to the pressure forces placed on the outside of the evacuated tube. A 68-cm- (27-in.)-diagonal tube was analyzed with and without an implosion protection band. The implosion protection band reduces the overall stresses in the tube and, in the event of an implosion, also contains the glass particles within the enclosure. Stress analysis (Fig 13) showed compressive stresses on the front face and tensile stresses on the sides of the tube. The implosion band reduced the maximum principal stress by 20%. Reliability analysis with CARES/*Life* showed that the implosion protection band significantly reduced the probability of failure to about 5×10^{-5}.

The structural integrity of a silicon carbide convective air-heater for use in an advanced power generation system has been assessed by ORNL and the NASA-Lewis Research Center. The design used a finned tube arrangement 1.8 m (70.9 in.) in length with 2.5-cm (1 in.)diameter tubes. Incoming air was to be heated from 390°C to 700°C (734°F to 1292°F). The hot gas flow across the tubes was at 980°C (1796°F). Heat transfer and stress analyses revealed that maximum stress gradients across the tube wall nearest the incoming air would be the most likely source of failure.

At the University of Florida College of Dentistry, probabilistic design techniques are being applied to dental ceramic crowns, as illustrated in Fig 14. Frequent failure of some ceramic crowns (e.g. 35% failure of molar crowns after three years), which occurs because of residual and functional stresses, necessitates design modifications and improvement of these restorations. The University of Florida is investigating thermal tempering treatment as a means of introducing compressive stresses on the surface of dental ceramics to improve the resistance to failure (Ref 93). Evaluation of the risk of material failure must be considered not only for the service environment but also from the tempering process.

REFERENCES

1. C.A. Johnson and W.T. Tucker, "Advanced Statistical Concepts of Fracture in Brittle Materials," in *Engineered Materials Handbook Volume 4 Ceramics and Glasses*, S. Snyder, tech. Chair, ASM, Materials Park, Ohio, 1991, pp. 708-715

2. W.A. Weibull, "The Phenomenon of Rupture in Solids," Ingenoirs Vetenskaps Akadanien Handlinger, 1939, No. 153

3. C.A. Johnson, "Fracture Statistics of Multiple Flaw Populations," in *Fracture Mechanics of Ceramics*, Vol. 5, eds. R.C. Bradt, A.G. Evans, D.P.H. Hasselman, and F.F. Lange, Plenum Press, New York-London, 1983, pp. 365-386

4. W.A. Weibull, "A Statistical Distribution Function of Wide Applicability," J. Appl. Mech., vol. 18, no. 3, Sept. 1951, pp. 293–297

5. F.T. Pierce, "The Weakest Link" Theorems of the Strength of Long and of Composite Specimens. Text. Inst. J., vol. 17, 1926, pp. T355–T368

6. T.A. Kontorova, "A Statistical Theory of Mechanical Strength," J. Tech. Phys (USSR), vol. 10, 1940, pp. 886–890

7. J.I. Frenkel and T.A. Kontorova, "A Statistical Theory of the Brittle Strength of Real Crystals," J. Phys. USSR, vol. 7, no. 3, 1943, pp. 108–114

8. J. Hu, "Modeling Size Effects and Numerical Techniques in Structural Reliability Analysis," Masters Thesis, Cleveland State University, 1994

9. T.T. Shih, "An Evaluation of the Probabilistic Approach to Brittle Design," Eng. Fract. Mech., vol. 13, no. 2, 1980, pp. 257–271

10. S.F. Duffy and S.M. Arnold, "Noninteractive Macroscopic Statistical Failure Theory for Whisker Reinforced Ceramic Composites," *Journal of Composite Materials*, vol. 24, no. 3, 1990, pp. 293-308

11. S.F. Duffy and J.M. Manderscheid, "Noninteractive Macroscopic Reliability Model for Ceramic Matrix Composites with Orthotropic Material Symmetry," *Journal of Engineering for Gas Turbines and Power*, vol. 112, no. 4, 1990, pp. 507-511

12. N.N. Nemeth, J.M. Manderscheid, and J.P.Gyekenyesi, "Ceramics Analysis and Reliability Evaluation of Structures (CARES) Users and Programmers Manual," NASA TP-2916, 1990

13. Gross, and J.P. Gyekenyesi, "Weibull Crack Density Coefficient for Polydimensional Stress States," J. Am. Ceram. Soc., vol. 72, no. 3, 1989, pp. 506–507

14. R.L. Barnett, C.L. Connors, P.C. Hermann, and J.R. Wingfield, "Fracture of Brittle Materials Under Transient Mechanical and Thermal Loading," U.S. Air Force Flight Dynamics Laboratory. AFFDL-TR-66-220, Mar. 1967

15. A.M. Freudenthal, "Statistical Approach to Brittle Fracture. Fracture, An Advanced Treatise," in Vol. 2, Mathematical Fundamentals, H. Liebowitz, ed., Academic Press, 1968, pp. 591–619

16. J. Margetson, "A Statistical Theory of Brittle Failure for an Anisotropic Structure Subjected to a Multiaxial Stress State," AIAA Paper 76-632, July 1976

17. A. Paluszny and W. Wu, "Probabilistic Aspects of Designing with Ceramics," J. Eng. Power, vol. 99, no. 4, Oct. 1977, pp. 617–630

18. G.J. DeSalvo, "Theory and Structural Design Application of Weibull Statistics," WANL-TME-2688, Westinghouse Astronuclear Lab., 1970

19. J.L. Wertz and P.W. Heitman, "Predicting the Reliability of Ceramic Turbine Components. Advanced Gas Turbine Systems for Automobiles," SAE-SP-465, Society of Automotive Engineers, 1980, pp. 69–77.

20. W.H. Dukes, "Handbook of Brittle Material Design Technology," AGARDograph 152, AGARD, Paris, France, 1971

21. S.B. Batdorf, "Fundamentals of the Statistical Theory of Fracture," *Fracture Mechanics of Ceramics*, Vol. 3, eds., Bradt, R. C., Hasselman, D. P. H. and Lange, F. F., Plenum Press, New York (1978), pp 1-30

22. Batdorf and J.G. Crose, "A Statistical Theory for the Fracture of Brittle Structures Subjected to Nonuniform Polyaxial Stresses," *Journal of Applied Mechanics*, Vol. 41, No. 2, June 1974, pp 459-464

23. Giovan and G. Sines, "Biaxial and Uniaxial Data for Statistical Comparison of a Ceramic's Strength," J. Am. Ceram. Soc., vol. 62, no. 9, Sept. 1979, pp. 510–515

24. M.G. Stout and J.J. Petrovic, "Multiaxial Loading Fracture of AL_2O_3 Tubes: I, Experiments," J. Am. Ceram. Soc., vol. 67, no. 1, Jan. 1984, pp. 14–18

25. J.J Petrovic and M.G. Stout, "Multiaxial Loading Fracture of Al_2O_3 Tubes: II, Weibull Theory and Analysis," J. Am. Ceram. Soc., vol. 67, no. 1, Jan., 1984, pp. 18–23

26. K. Palaniswamy and W.G. Knauss, "On the Problem of Crack Extension in Brittle Solids Under General Loading," Mech. Today, 1978, vol. 4, pp. 87–148.

27. D.K. Shetty, "Mixed-Mode Fracture Criteria for Reliability Analysis and Design with Structural Ceramics," J. Eng. Gas Turbines Power, vol. 109, no. 3, July 1987, pp. 282–289

28. S.F. Duffy, L.M. Powers, and A. Starlinger, "Reliability Analysis of Structural Components Fabricated from Ceramic Materials Using a Three-Parameter Weibull Distribution," *Transactions of the ASME - Journal of Engineering for Gas Turbines and Power*, Vol. 115, No. 1, pp. 109-116, January, 1993

29. G.D. Quinn, "Flexure Strength of Advanced Ceramics - A Round Robin Exercise," MTL TR-89-62 (Avail. NTIS, AD-A212101, 1989)

30. M.R. Foley, V.K. Pujari, L.C. Sales, and D.M. Tracey, "Silicon Nitride Tensile Strength Data Base from Ceramic Technology Program for Reliability Project," in *Life Prediction Methodologies and Data for Ceramic Materials*, eds. C.R. Brinkman and S.F. Duffy (ASTM, to be published)

31. L.-Y. Chao and D.K. Shetty, "Reliability Analysis of Structural Ceramics Subjected to Biaxial Flexure," *J. Am. Ceram. Soc.*, 74 [2]: 333-344 (1991)

32. S.F. Duffy, J.L. Palko, and J.P. Gyekenyesi, "Structural Reliability of Laminated CMC Components," *Transactions of the ASME - Journal of Engineering for Gas Turbines and Power*, Vol. 115, No. 1, pp. 103-108, 1993

33. D.J. Thomas and R.C. Wetherhold, "Reliability of Continuous Fiber Composite Laminates," *Comp. Struct.*, 17: 277-293 (1991).

34. J.L. Palko, "An Interactive Reliability Model for Whisker-Toughened Ceramics," Masters Thesis, Cleveland State University, 1992

35. Margetson and N.R. Cooper, "Brittle Material Design Using Three Parameter Weibull Distributions," in the *Proceedings of the IUTAM Symposium on Probabilistic Methods in the Mechanics of Solids and Structures*, eds. S. Eggwertz and N.C. Lind, Springer-Verlag, Berlin, pp. 253-262, 1984

36. Pai and J.P. Gyekenyesi, "Calculation of the Weibull Strength Parameters and Batdorf Flaw Density Constants for Volume and Surface-Flaw-Induced Fracture in Ceramics," NASA TM-100890, 1988

37. J.P Gyekenyesi and N.N. Nemeth, "Surface Flaw Reliability Analysis of Ceramic Components with the SCARE Finite Element Postprocessor Program," J. Eng. Gas Turbines Power, vol. 109, no. 3, July 1987, pp. 274–281

38. Gyekenyesi, J.P.: SCARE: A Postprocessor Program to MSC/NASTRAN for the Reliability Analysis of Structural Ceramic Components. J. Eng. Gas Turbines Power, vol. 108, no. 3, July 1986, pp. 540–546

39. J.C Cuccio, P. Brehm, H.T. Fang, J. Hartman, W. Meade, M.N. Menon, A. Peralta, J.Z. Song, T. Strangman, J. Wade, J. Wimmer, and D.C. Wu, "Life Prediction Methodology for Ceramic Components of Advanced Heat Engines, Phase I," ORNL/Sub/89-SC674/1/V1, Volume 1, Final Report, March, 1995

40. J.C Cuccio, P. Brehm, H.T. Fang, J. Hartman, W. Meade, M.N. Menon, A. Peralta, J.Z. Song, T. Strangman, J. Wade, J. Wimmer, and D.C. Wu, "Life Prediction Methodology for Ceramic Components of Advanced Heat Engines, Phase I," ORNL/Sub/89-SC674/1/V2, Volume 2, Final Report, March, 1995

41. C. Baker and D. Baker, "Design Practices for Structural Ceramics in Automotive Turbocharger Wheels", Engineered Materials Handbook, Volume 4: Ceramics and Glasses, ASM International, 1991, pp.722-727

42. C.J. Poplawsky, L. Lindberg, S. Robb, and J. Roundy, "Development of an Advanced Ceramic Turbine Wheel for an Air Turbine Starter," SAE Paper 921945, Presented at Aerotech '92, Anaheim, California, October 5-8, 1992

43. J.H. Selverian, d. O'Neil, and S. Kang, "Ceramic-to-Metal Joints: Part I-Joint Design," *American Ceramic Society Bulletin*, Vol. 71, No. 9, pp. 1403-1409, 1992

44. J.H. Selverian and S. Kang, "Ceramic-to-Metal Joints: Part II-Performance and Strength Prediction," *American Ceramic Society Bulletin*, Vol. 71, No. 10, pp. 1511-1520, 1992

45. C.L. Snydar, "Reliability Analysis of a Monolithic Graphite Valve," Presented at the 15th Annual Conference on Composites, Materials, and Structures, Cocoa Beach, FL, 1991

46. J.A. Salem, J.M. Manderscheid, M.R. Freedman, and J.P. Gyekenyesi, "Reliability Analysis of a Structural Ceramic Combustion Chamber," ASME Paper 91-GT-155, Presented at the International Gas Turbine and Aeroengine Congress and Exposition, Orlando, Florida, June 3-6, 1991

47. R.R. Wills, and R.E. Southam, "Ceramic Engine Valves," *Journal of the American Ceramic Society*, Vol. 72, No. 7, pp. 1261-1264, 1989

48. J.R. Smyth, R.E. Morey, and R.W. Schultz, "Ceramic Gas Turbine Technology Development and Applications," ASME Paper 93-GT-361, Presented at the International Gas Turbine and Aeroengine Congress and Exposition, Cincinnati, Ohio, May 24-27, 1993

49. G.D. Quinn, "Fracture Mechanism Maps For Advanced Structural Ceramics: Part 1; Methodology and Hot-Pressed Silicon Nitride Results," *Journal of Materials Science*, Vol. 25, 1990, pp. 4361-4376.

50. N.N. Nemeth, L.M. Powers, L.A. Janosik, and J.P Gyekenyesi, "CARES/Life Prediction Program (CARES/*Life*) Users and Programmers Manual," NASA TM-106316, to be puiblished

51. T.-J. Chuang, and S.F. Duffy, "A Methodology to Predict Creep Life for Advanced Ceramics Using Continuum Damage Mechanics," *Life Prediction Methodologies and Data for Ceramic Materials, ASTM STP 1201*, C.R. Brinkman and S.F. Duffy, Eds., American Society for Testing and Materials, Philadelphia, 1994, pp. 207-227

52. Y. Corapcioglu, and T. Uz, "Constitutive Equations for Plastic Deformation of Porous Materials," *Powder Technology*, Vol. 21, 1978, pp. 269-274

53. H.A. Kuhn, and C.L Downey, C.L., "Deformation Characteristics and Plasticity Theory of Sintered Powder Metals," *International Journal of Powder Metallurgy*, Vol. 7, 1971, pp. 15-25

54. S. Shima, and M. Oyane, "Plasticity Theory for Porous Metals," *International Journal of Mechanical Sciences*, Vol. 18, 1976, pp. 285

55. R.J. Green, "A Plasticity Theory for Porous Solids," *International Journal for Mechanical Sciences*, Vol. 14, 1972, pp. 215

56. A.L. Gurson, "Continuum Theory of Ductile Rupture by Void Nucleation and Growth: Part I¼Yield Criteria and Flow Rules for Porous Ductile Media," *Journal of Engineering Materials and Technology*, Vol. 99, 1977, pp. 2-15

57. M.E. Mear, and J.W. Hutchinson, "Influence of Yield Surface Curvature on Flow Localization in Dilatant Plasticity," *Mechanics of Materials*, Vol. 4, 1985, pp. 395-407

58. J.-L. Ding, K.C. Liu, and C.R. Brinkman, "A Comparative Study of Existing and Newly Proposed Models for Creep Deformation and Life Prediction of Si3N4," in *Life Prediction Methodologies and Data for Ceramic Materials, ASTM STP 1201*, C.R. Brinkman and S.F. Duffy, Eds., American Society for Testing and Materials, Philadelphia, 1994, pp. 62-83

59. C.S. White, and R.M. Hazime, "Internal Variable Modeling of the Creep of Monolithic Ceramics," Proceedings of the 11th Biennial Conference on Reliability, Stress Analysis, and Failure Prevention, O. Jadaan, ed., The American Society of Mechanical Engineers, Philadelphia,1995

60. K.C. Liu, C.R. Brinkman, J.-L. Ding, and S. Liu, "Predictions of Tensile Behavior and Strengths of Si_3N_4 Ceramic at High Temperatures Based on a Viscoplastic Model," ASME Transactions,1995, 95-GT-388

61. D.N. Robinson, "A Unified Creep-Plasticity Model for Structural Metals at High Temperature," ORNL/TM 5969, 1978.

62. S.F. Duffy, "A Unified Inelastic Constitutive Theory for Sintered Powder Metals," *Mechanics of Materials*, Vol. 7, 1988, pp. 245-254

63. K.J. Willam, and E.P. Warnke, "Constitutive Model for the Triaxial Behaviour of Concrete, *Int. Assoc. Bridge Struct. Eng. Proc.*, Vol. 19, 1975, pp. 1-30

64. L.A. Janosik and S.F. Duffy, "A Viscoplastic Constitutive Theory for Monolithic Ceramic Materials-I," *Proceedings of the Physics and Process Modeling (PPM) and Other Propulsion R&T Conference, Volume I: Materials Processing, Characterization, and Modeling; Lifing Models*, NASA CP-10193, 1997, Paper 15

65. L.A. Janosik, and S.F. Duffy, "A Viscoplastic Constitutive Theory for Monolithic Ceramics - I," *Transactions of the ASME Journal of Engineering for Gas Turbines and Power*, Paper No. 96-GT-368. Presented at the ASME International Gas Turbine Congress, Exposition, and Users' Symposium, Birmingham, UK, June 10-13, 1996

66. J.R. Rice, "On the Structure of Stress-Strain Relations for Time-Dependent Plastic Deformation in Metals," *Journal of Applied Mechanics*, 37, 1970, pp. 728

67. A.R.S. Ponter, and F.A. Leckie, "Constitutive Relationships for Time-Dependent Deformation of Metals," *ASME Journal of Engineering Materials and Technology*, Vol. 98, 1976

68. L.A. Janosik, "A Unified Viscoplastic Constitutive Theory for Monolithic Ceramics," Master's Thesis, Cleveland State University, Cleveland, OH, 1997, to be published

69. E.C. Bingham, *Fluidity and Plasticity*, McGraw-Hill, New York, 1922

70. K. Hohenemser, and W. Prager, "Ueber die Ansaetze der Mechanik Isotroper Kontinua," *Zeit fuer angewandte Mathematik und Mechanik*, Vol. 12, 1932

71. A.G. Evans, and S.M. Wiederhorn, "Crack Propagation and Failure Prediction in Silicon Nitride at Elevated Temperatures", *Journal of Material Science*, Vol. 9, 1974, pp 270-278

72. S.M. Wiederhorn, and E.R. Fuller, Jr, Structural Reliability of Ceramic Materials, *Materials Science and Engineering*, vol. 71, 1985, pp. 169–186

73. S.M. Wiederhorn, E.R. Fuller, and R. Thomson, Micromechanisms of Crack Growth in Ceramics and Glasses in Corrosive Environments, *Metal Science*, Aug.-Sept. 1980, pp. 450–458

74. S.M. Wiederhorn, *Fracture Mechanics of Ceramics*, R.C. Bradt, D.P. Hasselman, and F.F. Lange, eds., Plenum, New York, 1974, pp. 613-646

75. P. Paris, and F. Erdogan, "A Critical Analysis of Crack Propagation Laws", *Journal of Basic Engineering*, Vol. 85, 1963, pp. 528-534

76. K. Walker, "The Effect of Stress Ratio During Crack Propagation and Fatigue for 2024-T3 and 7075-T6 Aluminum", ASTM STP 462, 1970, pp. 1-14

77. R.H. Dauskardt, M.R. James, J.R. Porter, and R.O. Ritchie, "Cyclic Fatigue Crack Growth in SiC-Whisker-Reinforced Alumina Ceramic Composite: Long and Small Crack Behavior", *Journal of the American Ceramic Society*, Vol. 75, No. 4, 1992, pp 759-771

78. P.C. Paris, and G.C. Sih, Stress Analysis of Cracks. ASTM STP 381, 1965, pp. 30-83

79. T. Thiemeier, "Lebensdauervorhersage fun Keramische Bauteile Unter Mehrachsiger Beanspruchung", Ph.D. dissertation, University of Karlesruhe, Germany, 1989

80. G. Sturmer, A. Schulz, and S. Wittig, "Lifetime Prediction for Ceramic Gas Turbine Components", ASME Preprint 91-GT-96, June 3-6, 1991

81. F. Lange, "Interrelations Between Creep and Slow Crack Growth for Tensile Loading Conditions," *International Journal of Fracture*, Vol. 12, pp. 739-744, 1976

82. S.F. Duffy, and J.P. Gyekenyesi, "Time Dependent Reliability Model Incorporating Continuum Damage Mechanics for High-Temperature Ceramics," NASA TM-102046, May 1989

83. L.M. Kachanov, "Time of the Rupture Process Under Creep Conditions," *Izv. Akad. Nauk. SSR, Otd Tekh. Nauk* 8, 26, 1958

84. F.A. Leckie, "Advances in Creep Mechanics," *Creep in Structures*, A.R.S. Ponter, and D.R. Hayhurst, eds., Springer-Verlag, Berlin, 1981, p. 13

85. K. Jakus, D.C. Coyne, and J.E. Ritter, "Analysis of Fatigue Data for Lifetime Predictions for Ceramic Materials," *Journal of Material Science*, Vol. 13, 1978, pp. 2071-2080

86. J.R. Smyth, R.E. Morey, and R.W. Schultz, "Ceramic Gas Turbine Technology Development and Applications", ASME Paper 93-GT-361, Presented at the International Gas Turbine and Aeroengine Congress and Exposition, Cincinnati, Ohio, May 24-27, 1993

87. S.G. Berenyi, S.J. Hilpisch, and L.E. Groseclose, "Advanced Turbine Technology Applications Project (ATTAP)", Proceedings of the Annual Automotive Technology Development Contractor's Coordination Meeting, Dearborn, Michigan, October 18-21, 1993. SAE International, Warrendale, PA

88. D.R. Johnson, and R.B. Schultz, "The Ceramic Technology Project: Ten Years of Progress", ASME Paper 93-GT-417, Presented at the International Gas Turbine and Aeroengine Congress and Exposition, Cincinnati, Ohio, May 24-27, 1993

89. J. Cuccio, "Life Prediction Methodology for Ceramic Components of Advanced Heat Engines", Proceedings of the Annual Automotive Technology Development Contractor's Coordination Meeting, Dearborn, Michigan, October 18-21, 1993

90. P.K. Khandelwal, N.J. Provenzano, and W.E. Schneider, "Life Prediction Methodology for Ceramic Components of Advanced Vehicular Engines", Proceedings of the Annual Automotive Technology Development Contractor's Coordination Meeting, Dearborn, Michigan, October 18-21, 1993

91. M. van Roode, W.D. Brentnall, P.F. Norton, and G.P. Pytanowski, "Ceramic Stationary Gas Turbine Development", ASME Paper 93-GT-309, Presented at the International Gas Turbine and Aeroengine Congress and Exposition, Cincinnati, Ohio, May 24-27, 1993

92. Ghosh, C.Y. Cha, W. Bozek, and S. Vaidyanathan, "Structural Reliability Analysis of CRTs", *Society for Information Display International Symposium Digest of Technical Papers Volume XXIII*, Hynes Convention Center Boston, Massachusetts, May 17-22, 1992. Society ofInformation Dsiplay, Playa Del Ray, CA, pp. 508-510

93. Hojjatie, "Thermal Tempering of Dental Ceramics", *Proceedings of the ANSYS Conference and Exhibition*, Vol. 1, Swanson Analysis Systems Inc., Houston, PA, pp. I.73-I.91, 1992

Table 1 Alumina Fracture Stress Data Utilized in Nonlinear Regression Estimation

Specimen	Stress	Specimen	Stress	Specimen	Stress
1	307 *MPa*	13	347 *MPa*	25	376 *MPa*
2	308 *MPa*	14	350 *MPa*	26	376 *MPa*
3	322 *MPa*	15	352 *MPa*	27	381 *MPa*
4	328 *MPa*	16	353 *MPa*	28	385 *MPa*
5	328 *MPa*	17	355 *MPa*	29	388 *MPa*
6	329 *MPa*	18	356 *MPa*	30	395 *MPa*
7	331 *MPa*	19	357 *MPa*	31	402 *MPa*
8	332 *MPa*	20	364 *MPa*	32	411 *MPa*
9	335 *MPa*	21	371 *MPa*	33	413 *MPa*
10	337 *MPa*	22	373 *MPa*	34	415 *MPa*
11	343 *MPa*	23	374 *MPa*	35	456 *MPa*
12	345 *MPa*	24	375 *MPa*		

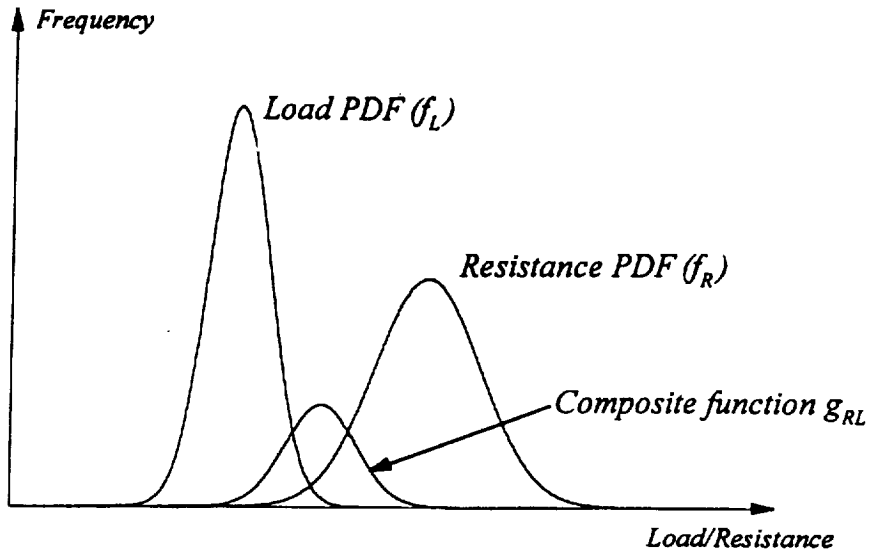

Fig 1 Interference Plot for Load and Resistance Random Variables

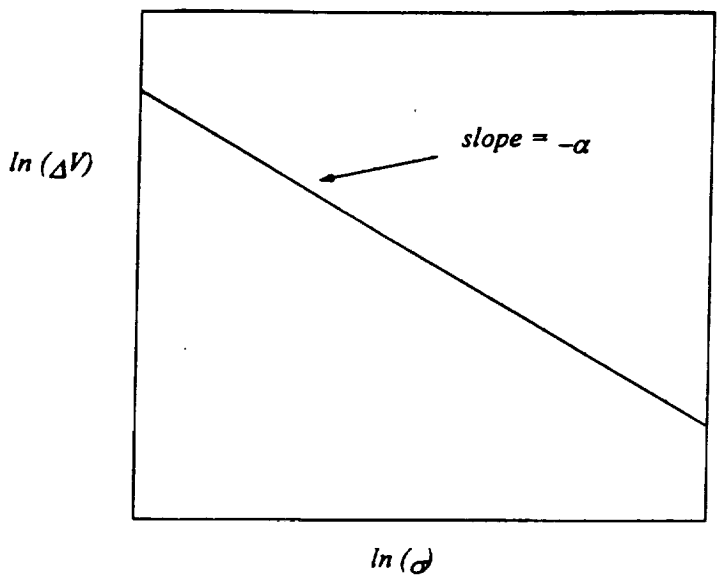

Fig 2 Specimen gage volume plotted as a function of failure stress

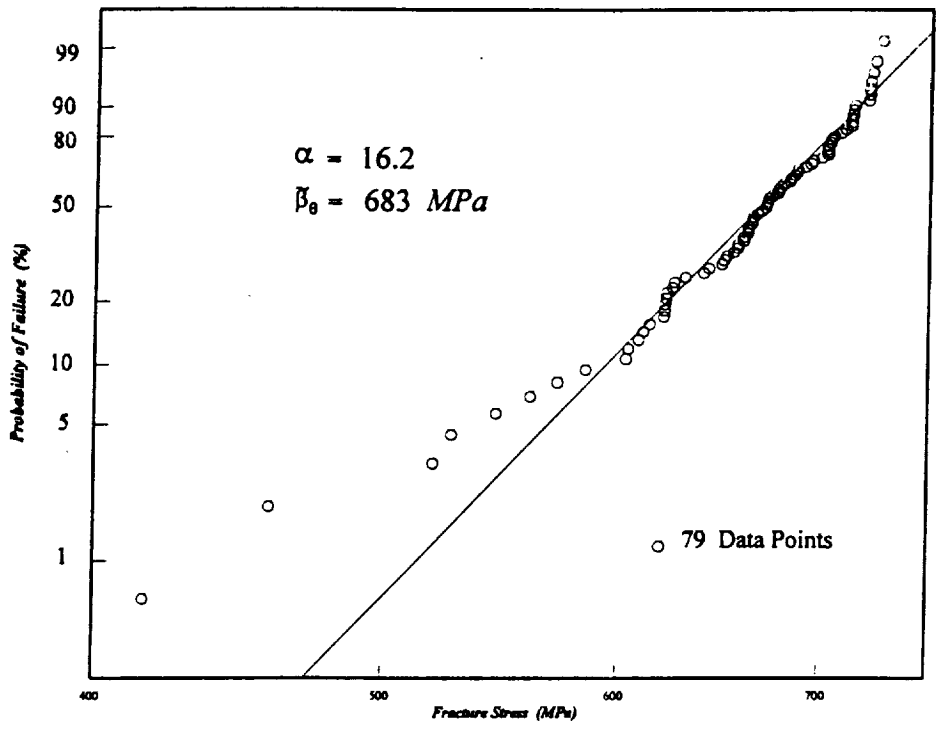

Fig 3 Sample with multiple failure populations.

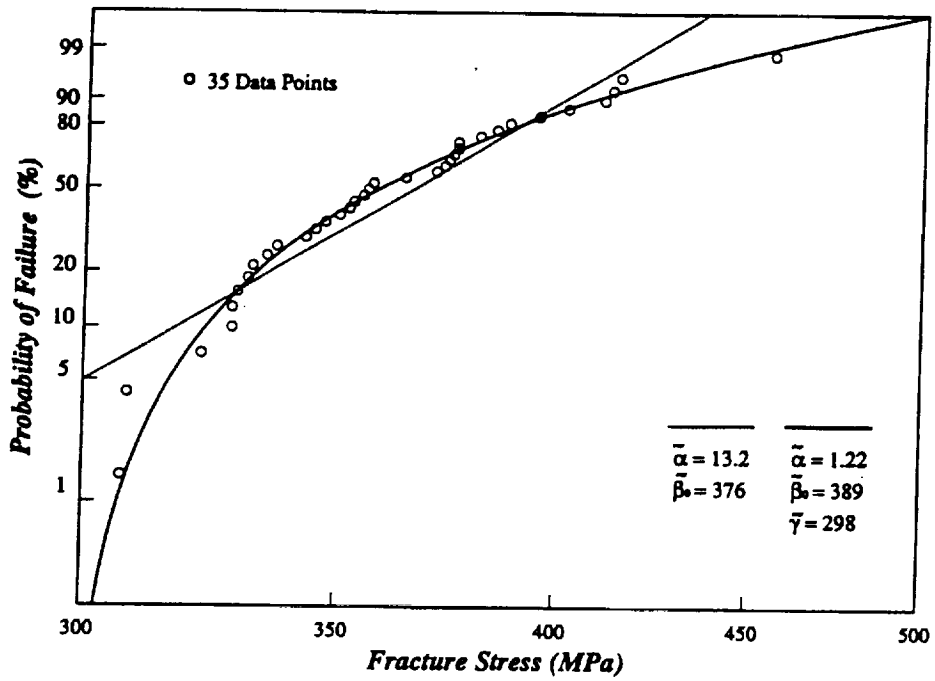

Fig 4 Alumina failure data (see Table 1) and probability of failure curves based on estimated parameters for the two- and three-parameter Weibull distributions.

Fig 5 Ceramic automotive turbocharger wheel.
(Picture provided courtesy of AlliedSignal Turbocharging and Truck Brake Systems.)

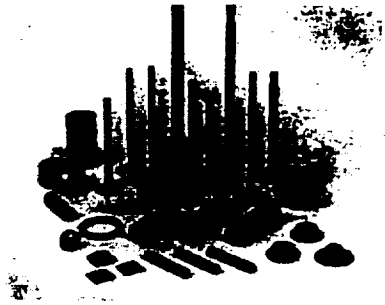

Fig 6 Automotive valves and engine components.
(Picture provided courtesy of TRW Automotive valve Division.)

Fig 7 The largest known ZnSe window manufactured for a cryogenic vacuum chamber.
(Picture provided courtesy of Hughes Danbury Optical Systems.)

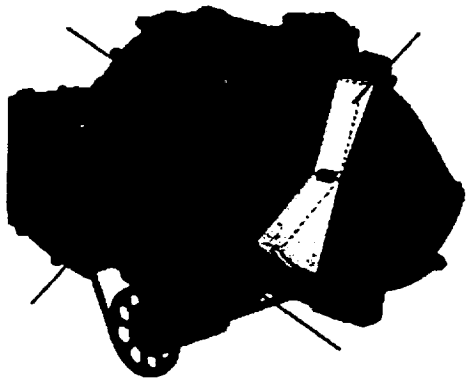


Scroll


Combustor

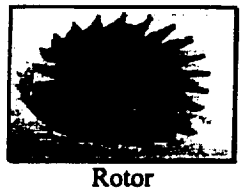
Rotor

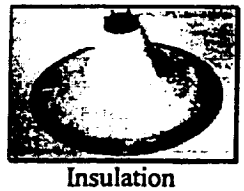
Insulation

Fig 8 Gas turbine engine and components.
(Pictures provided courtesy of Allison Engine Company.)

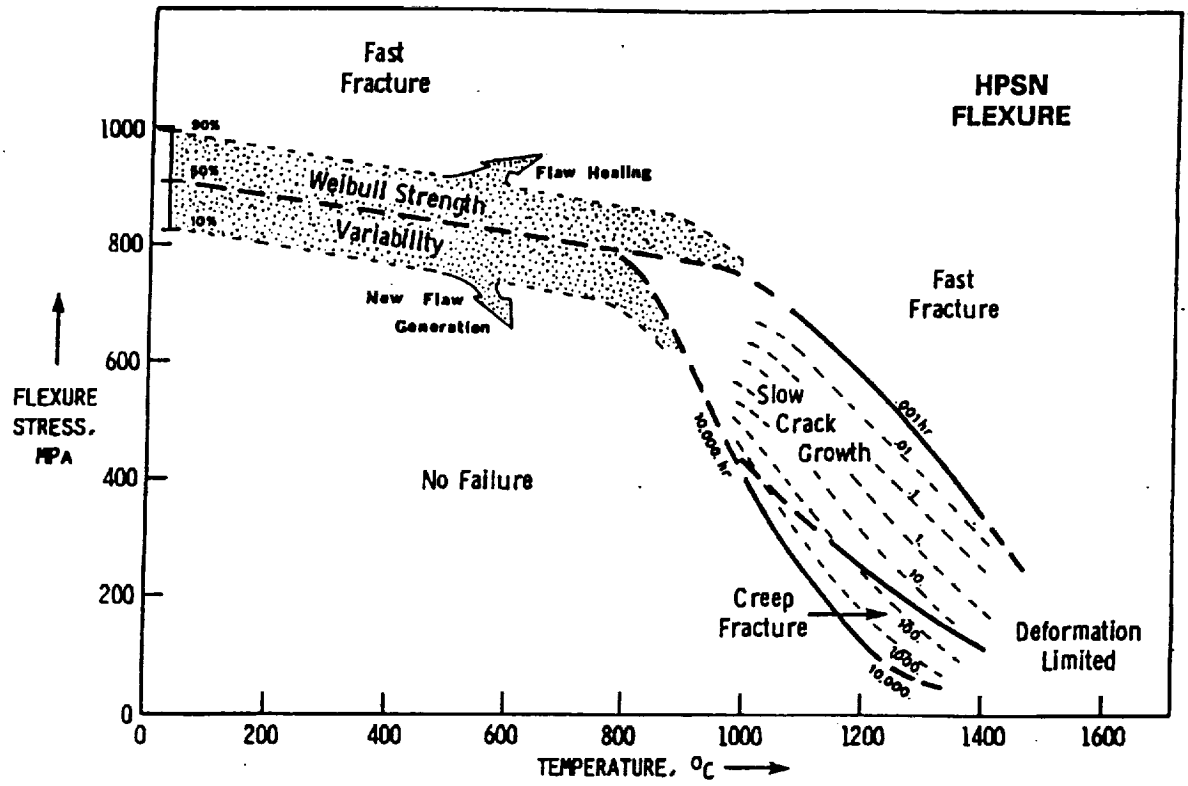

Fig 9 Fracture mechanism map for hot-pressed silicon nitride flexure bars. Fracture mechanism maps help illustrate the relative contribution of various failure modes as a function of temperature and stress. Source: Ref 49

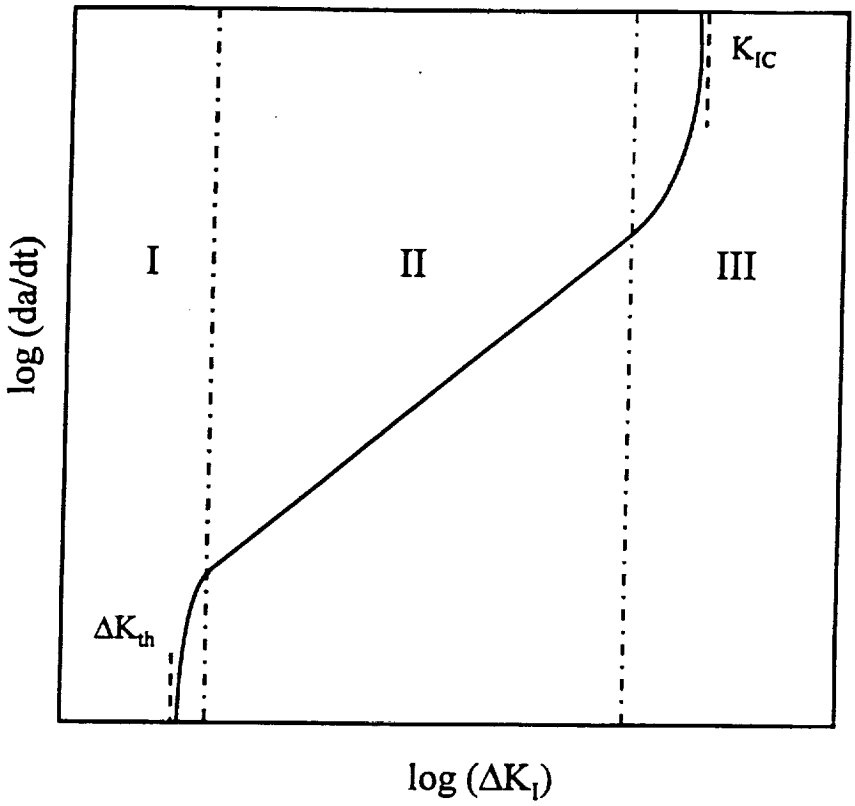

Fig 10 Schematic illustrating three different regimes of crack growth.

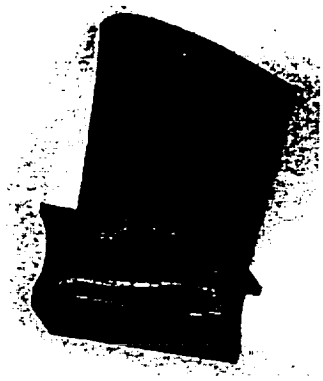

Fig 11 Stress contour plot of first-stage silicon nitride turbine rotor blade for a natural-gas-fired industrial turbine engine for cogeneration. The blade is rotating at 14,950 rpm.
(Picture provided courtesy of Solar Turbines Incorporated.)

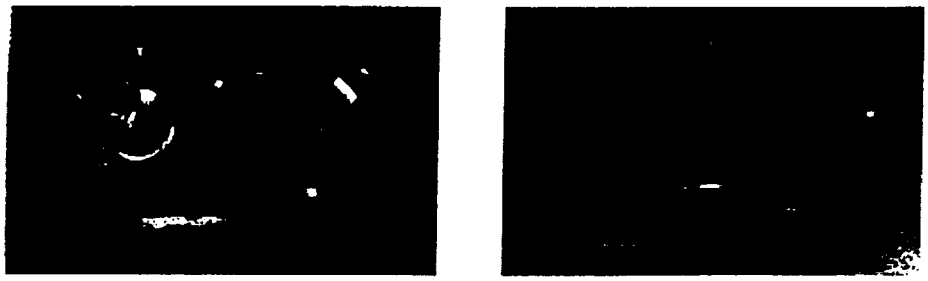

Fig 12 (Left) Ceramic turbine wheel and nozzle for advanced auxiliary power unit.
(Right) Ceramic components for small expendable turbojet.
(Pictures provided courtesy of Sundstrand Aerospace Corporation.)

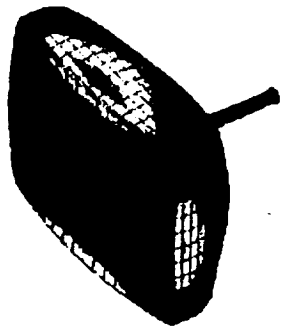

Fig 13 Stress plot of an evacuated 68-cm- (27-in.)-diagonal cathode ray tube (CRT). The probability of failure calculated with CARES/*Life* was less than 5.0×10^{-5}. (Picture provided courtesy of Philips Display Components Company.)

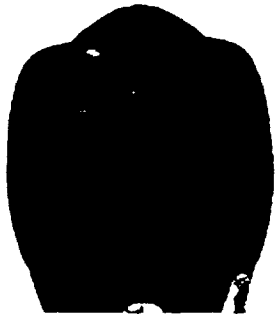

Fig 14 Stress contour plot of ceramic dental crown, resulting from a 600 N biting force.
(Picture provided courtesy of University of Florida College of Dentistry.)